Results in Control and Optimization 22 (2026) 100664

Contents lists available at ScienceDirect

Results in Control and Optimization

journal homepage: www.elsevier.com/locate/rico

Sustainable wind farm layout design for maximizing power output and reducing environmental impact

Khamiss Cheikh [a,*], EL Mostapha Boudi [a], Rabi Rabi [b], Hamza Mokhliss [c]

[a] Department of Mechanical Engineering, Energetic team, Mechanical and Industrial Systems (EMISys), Mohammadia School of Engineers, Mohammed V University, Rabat, Morocco
[b] Department of Physics (LPM-ERM), Faculty of Sciences and Techniques, Sultan Moulay Sliman University, B.P.523, 23000 Beni-Mellal, Morocco
[c] Department of Physics, Laboratory of Electronics, Instrumentation and Energetics, Faculty of Sciences, Chouaib Doukkali University, El Jadida, Morocco

ARTICLE INFO

Keywords:
Wind farm layout optimization
Multi-objective optimization
Wake modeling
Turbulence intensity
Stochastic wind fields
Renewable energy systems

ABSTRACT

Wind farm layout design continues to face methodological constraints that limit its applicability under realistic operating conditions. Existing approaches frequently rely on single-objective formulations that prioritize either energy maximization or wake-loss reduction, thereby failing to capture the interdependent trade-offs among power generation, turbulence intensity, and wake-induced performance degradation. In addition, widely adopted wake models often use simplified aerodynamic representations that overlook turbine–turbine coupling effects, while deterministic wind-field assumptions ignore the stochastic variability in wind speed and direction that critically influences wake propagation. These limitations underscore the need for a more comprehensive and physically grounded optimization strategy. This study proposes a tailored multi-objective optimization framework that integrates analytical wake modeling with stochastic environmental characterization to identify efficient turbine placements within the farm boundary. The method concurrently optimizes power output, turbulence attenuation, and wake-related energy deficits while enforcing spatial and operational constraints. Numerical evaluations demonstrate marked performance improvements relative to baseline configurations. Turbines situated in favorable aerodynamic regions (*T4* and *T5*) achieve power outputs of *1.84–1.89 MW*, representing an increase of up to *72%* compared to downstream turbines subjected to wake interference (*1.03–1.13 MW*). Turbulence intensity decreases by more than *55%* (*1.20–1.28* versus *2.58–2.81*), and wake-related energy losses are reduced by over *60%* (*0.0065–0.0072* versus *0.013–0.017*). These quantitative gains confirm the efficacy of the proposed optimization framework and highlight its potential for scalability, enhanced aerodynamic fidelity, and integration into future large-scale wind-farm planning and operational decision-support systems.

1. Introduction

The global transition toward low-carbon energy systems has heightened the strategic importance of wind power as a reliable and scalable renewable resource [1,2]. Substantial progress in turbine aerodynamics, control systems, and digital monitoring has enabled modern wind farms to achieve unprecedented levels of operational sophistication [3,4]. Yet, maximizing the energy yield of a wind

* Corresponding author.
E-mail address: khamiss_cheikh@um5.ac.ma (K. Cheikh).

https://doi.org/10.1016/j.rico.2026.100664
Received 23 September 2025; Received in revised form 28 December 2025; Accepted 25 January 2026
Available online 26 January 2026

farm remains a complex engineering undertaking governed by the interplay between aerodynamic interactions, environmental variability, and system-level constraints. Recent studies, such as Sorkhabi et al. [5], have considered additional constraints, such as land use and noise, in multi-objective wind farm layout optimization, offering a more comprehensive framework to improve layout efficiency while minimizing environmental impact. Within this context, two distinct research domains have emerged as central to wind farm performance enhancement: wind farm layout optimization and wind farm control optimization [6,7]. Although both pursue the overarching goal of maximizing energy capture, they differ fundamentally in their design variables, temporal scales, and methodological requirements [8,9].

Wind farm layout optimization focuses on determining the spatial configuration of turbines within the project site prior to construction [10–12]. Several studies have developed optimization techniques to maximize energy capture in wind farms. Notably, Kusiak and Song [13] developed an approach to optimize turbine placement for maximum wind energy capture in wind farms. This design-stage decision dictates the aerodynamic environment in which all turbines operate, influencing wake formation, turbulence propagation, mechanical loading, and long-term energy production [14,15]. Wake interactions, caused by momentum deficits and turbulence generated by upstream turbines, are among the primary sources of efficiency loss [16,17]. They reduce the effective inflow velocity available to downstream machines and amplify dynamic loads, thereby accelerating fatigue and increasing maintenance costs [18,19]. Foundational studies have provided a detailed understanding of these aerodynamic mechanisms [20–22]. Wang [23] investigated turbine placement under irregular boundary conditions; Herbert-Acero et al. [24] surveyed methodological approaches to wake-aware farm design; Mahmoudi [25] validated wake modeling using thermofluid dynamic principles; and Ross and Altman [26] examined aerodynamic blockage effects with direct relevance to farm-wide design considerations. These contributions highlight the critical influence of spatial configuration on cumulative energy yield.

Complementing layout decisions, wind farm control optimization has evolved into a vibrant research field that aims to mitigate wake losses through real-time operational adjustments. Unlike layout optimization, which fixes the geometric structure of the farm, control optimization seeks to manipulate turbine yaw, pitch, and torque settings to redistribute wake interactions dynamically. Recent contributions have demonstrated the effectiveness of data-driven and model-free approaches. The multi-resolution optimized relative step-size random search method has shown the ability to increase farm-level power without relying on explicit wake models. Reinforcement learning combined with recursive least squares has exhibited strong performance in closed-loop wake steering under varying inflow conditions. Meanwhile, smoothed-functional-algorithm–optimized PID controllers have improved turbine speed regulation and mitigated cascade wake interactions. These studies underscore the growing maturity of control-oriented strategies for improving wind farm performance. Nevertheless, their efficacy is inherently constrained by the aerodynamic baseline established through turbine placement, reinforcing the foundational role of layout optimization.

Recent advancements in wind farm control have increasingly focused on mitigating wake-interaction losses through model-free and data-driven control strategies. In wind turbine performance simulations, Ji et al. [27] employed Lagrangian dynamic large-eddy simulation (LES) to model horizontal-axis tidal turbines, offering significant insights into wake dynamics and turbine performance. A first line of work introduces model-free wind farm power optimization using multi-resolution optimized relative step-size random search, demonstrating the capacity to increase farm-level production without explicit wake models. Complementary approaches rely on reinforcement-learning-based closed-loop control, where recursive least squares adaptation enables turbines to adjust yaw or torque settings in real time to counter evolving wake distortions [28]. Other contributions employ improved smoothed-functional-algorithm-optimized PID controllers to enhance rotor speed regulation and reduce wake-induced fluctuations, thereby stabilizing downstream flow conditions [29,30]. These studies collectively highlight the increasing maturity of control-oriented strategies for managing wake interactions and improving operational efficiency at the farm scale. They also underline that control optimization remains fundamentally constrained by the aerodynamic baseline imposed by turbine placement, reinforcing the central role of layout optimization.

Despite considerable advances, the optimization of entire wind farm layouts remains a multi-objective and nonlinear problem, complicated by wake interactions, turbulence generation, and stochastic environmental conditions. Traditional formulations typically focus on a single objective (most often maximizing energy or minimizing wake losses) which limits their ability to capture the inherent trade-offs between aerodynamic efficiency, mechanical loading, and energy losses. In response, recent research has incorporated more advanced optimization methods, including multi-objective evolutionary algorithms, surrogate-assisted frameworks, and reinforcement-learning–based spatial search techniques. Subramanian et al. [10] applied NSGA-III to evaluate wind energy potential under multiple criteria; Ma et al. [13] introduced hypervolume-improved evolutionary optimization for hybrid renewable energy systems; and Zhang et al. [17] demonstrated the effectiveness of multi-objective optimization in turbine control under complex dynamic conditions. While these approaches broaden the methodological landscape, many remain computationally intensive or rely on specialized assumptions that limit their practical applicability to layout optimization under realistic wind variability.

Parallel to these developments, recent literature has also highlighted the promise of single-agent optimization algorithms, including safe experimentation dynamics, memorizable smoothed functional algorithms, and norm-limited simultaneous perturbation stochastic approximation (SPSA). These techniques are well suited to online and real-time optimization tasks due to their low computational burden and fast convergence properties. However, they are inherently designed for scalar-objective optimization and do not naturally extend to the high-dimensional spatial search spaces or the multi-criteria aerodynamic trade-offs that characterize wind farm layout design. As such, they are effective in operational control but insufficient for comprehensive design-stage optimization [31].

In addition to these considerations, recent contributions have underscored the growing relevance of single-agent, model-free optimization schemes within wind farm control. Notable examples include Safe Experimentation Dynamics (SED) [32], the memorizable smoothed functional algorithm (MSFA) [33], and the norm-limited smoothed functional algorithm developed for advanced

controller tuning [34]. These approaches are well suited to low-dimensional, scalar-objective control problems and offer clear computational advantages in real-time operational settings. However, their conceptual formulation inherently limits them to single-objective performance metrics and prevents them from addressing the strongly coupled aerodynamic interactions that characterize wind farm layout design, including simultaneous trade-offs between power production, turbulence intensity, and wake-induced energy deficits. Consequently, their demonstrated effectiveness in operational control does not translate to the multi-objective, geometry-dependent nature of spatial layout optimization. This methodological limitation reinforces the need for a dedicated multi-objective framework capable of representing the full spectrum of aerodynamic interactions and constraint-driven spatial dependencies that govern wind farm layout performance.

To address the limitations of existing approaches, the present study introduces a custom multi-objective optimization framework tailored specifically to wind farm layout design. This framework integrates analytical wake modeling, stochastic wind-field representation, and a reward-based evaluation strategy to jointly assess power output, turbulence intensity, and wake-related energy deficits. By explicitly accounting for environmental stochasticity and aerodynamic coupling, the proposed approach provides a systematic and physically grounded means of identifying efficient turbine placements within the farm boundary.

The main contributions of this study are as follows:

- A comprehensive multi-objective optimization formulation integrating power output, turbulence intensity, and wake-induced energy deficits into a unified aerodynamic framework.
- A Reward-Guided Multi-Objective Stochastic Algorithm (RG-MOSA) capable of reconciling competing aerodynamic objectives while enforcing spacing and boundary constraints.
- A quantitative performance evaluation demonstrating measurable improvements in power production, turbulence reduction, and wake-loss mitigation relative to baseline layouts.

Recent offshore studies have highlighted that wake behavior and flow evolution over marine surfaces exhibit dynamics fundamentally different from those occurring over land [35]. For example, Kong et al. [36] quantified the pitch-induced response of side-by-side horizontal-axis tidal stream turbines in wave-current interactions, providing important insights into turbine performance under complex marine conditions. Marine atmospheric boundary layers are strongly influenced by sea-surface roughness, wave-induced airflow modulation, humidity gradients, and thermal stratification [37,38]. State-of-the-art investigations, including recent offshore LES–RANS hybrid analyses and full-scale wake measurements [39,40], have demonstrated that wave–wind coupling significantly alters wake recovery rates and turbulence generation in offshore environments [41,42]. Additional contributions from ocean engineering have examined the interaction between turbine wakes and ship-induced flow disturbances, low-level jet formation, and marine boundary-layer shear [43,44]. These interdisciplinary findings further justify the importance of incorporating marine fluid-dynamics principles into offshore wake modeling and motivate the future integration of high-fidelity CFD tools into the proposed optimization framework [45,46].

Additional recent studies have reinforced the importance of integrating aerodynamic, acoustic, and wake-dynamics considerations into wind farm layout design. Cao et al. [47] demonstrated that multi-criteria optimization (accounting simultaneously for power output, wake effects, and noise constraints) significantly improves the overall efficiency of wind energy conversion systems, highlighting the need for comprehensive aerodynamic–acoustic trade-off evaluation. Al-Addous et al. [48] showed that turbine spatial configuration strongly impacts the accuracy of predicted farm-level energy yield, reinforcing the critical role of optimized spacing and directional arrangement in layout planning. In parallel, high-fidelity fluid-dynamics investigations have provided deeper insights into wake formation and yaw-induced flow deformation. Ji et al. [49] examined wake evolution under yaw-offset conditions using advanced flow diagnostics, while Yin et al. [50] employed lattice-Boltzmann modeling to characterize wake behavior and performance sensitivity for ducted turbines. These contributions collectively highlight the complexity of wake interactions and the necessity of robust, physics-informed optimization methods such as the one proposed in this study.

The remainder of this paper is organized as follows. Section 2 presents the methodological formulation of the optimization framework. Section 3 details the simulation configuration and input parameters. Section 4 reports and analyzes the optimization results. Section 5 discusses engineering implications. Section 6 concludes the study and outlines perspectives for future work.

2. Methodology

2.1. Problem formulation

2.1.1. Multi-objective mathematical formulation

The problem of optimizing wind farm layouts involves maximizing the total power output while simultaneously minimizing the turbulence intensity and wake losses within the farm. This optimization is inherently multi-objective and non-linear, incorporating stochastic elements due to fluctuating wind conditions and the aerodynamic interactions between turbines.

In this study, we consider a wind farm consisting of $n=5$ turbines. The positions of each turbine T_i are represented by Cartesian coordinates (x_i,y_i), where $i\in\{1,2,\ldots,5\}$. The vector of decision variables representing the positions of all turbines is defined as [21]:

$$\mathbf{X} = \{(x_1,y_1),(x_2,y_2),\ldots,(x_5,y_5)\} \tag{1}$$

The multi-objective optimization problem can be expressed as [22]:

$$\min_{\mathbf{X}} \mathbf{F}(\mathbf{X}) = \begin{bmatrix} -f_1(\mathbf{X}) \\ f_2(\mathbf{X}) \\ f_3(\mathbf{X}) \end{bmatrix} \tag{2}$$

Where:

- $f_1(X)$ represents the total power output of the wind farm, which we aim to maximize (hence the negative sign in the formulation),
- $f_2(X)$ is the aggregate turbulence intensity across all turbines, which we seek to minimize, and
- $f_3(X)$ accounts for the wake losses, or energy deficits due to wake effects between turbines.

This optimization problem is subject to the following physical and operational constraints, which ensure the feasibility and practicality of the wind farm layout.

In order to ensure the turbine placement results in a viable and efficient layout, the optimization process must satisfy several physical constraints. These constraints define the feasible solution space and prevent the placement of turbines in configurations that would lead to suboptimal or infeasible solutions.

2.1.2. Minimum spacing constraint

To avoid mechanical failures and aerodynamic inefficiencies, it is necessary to maintain a minimum distance D_{min} between each pair of turbines. This constraint ensures that turbines are sufficiently spaced to minimize the effects of wake interference and mechanical loading. The minimum spacing constraint is given by [23]:

$$\| X_i - X_j \|^2 \geq D_{\min}^2, \forall i \neq j \tag{3}$$

Where:

- $\|X_i - X_j\|$ represents the Euclidean distance between turbines T_i and T_j.

The minimum spacing of *300 m* used in this study is consistent with standard offshore engineering guidelines for medium-to-large rotor diameters (*100–160 m*) and corresponds to approximately *2.5–3* rotor diameters, which is commonly adopted to limit direct wake overlap and excessive fatigue loading. This value also reflects practical offshore installation constraints, including foundation interaction distances, cabling corridors, and vessel maneuvering requirements. To assess the influence of the spacing parameter, a preliminary sensitivity evaluation was performed by varying the minimum permissible spacing between *240 m* and *480 m*. The analysis showed that reducing spacing below *300 m* leads to rapid increases in turbulence intensity and wake losses (particularly for downstream turbines) while larger spacings reduce aerodynamic interference but increase the geometric footprint and infrastructure length. These observations confirm that the selected *300 m* spacing represents a balanced compromise between aerodynamic efficiency and offshore installation feasibility.

2.1.3. Farm boundary constraint

In addition to the minimum spacing between turbines, each turbine must be located within the permissible boundaries of the wind farm. These boundaries are typically defined by a rectangular or polygonal region. The constraint is expressed as [24]:

$$\left(x_i^{\min}, y_i^{\min}\right) \leq (x_i, y_i) \leq \left(x_i^{\max}, y_i^{\max}\right), \quad \forall i \tag{4}$$

Where:

- $\left(x_i^{\min}, y_i^{\min}\right)$ and $\left(x_i^{\max}, y_i^{\max}\right)$ denote the minimum and maximum allowable positions for turbine T_i within the farm area.

2.1.4. Wake interference

Each turbine is affected by the wake produced by upstream turbines, which reduces the wind velocity at downstream turbines. The effective wind velocity at turbine T_i is reduced due to the wake effects of other turbines, as expressed by [25]:

$$V_i = V_0 \left(1 - \sum_{j \in W_i} \Delta V_{ij}\right) \tag{5}$$

Where:

- • V_i is the effective wind velocity at turbine T_i,
- • V_0 is the free-stream wind speed, and
- • ΔV_{ij} represents the velocity deficit caused by turbine T_j on turbine T_i, calculated as [26]:

$$\Delta V_{ij} = \left(\frac{D_r}{\| X_i - X_j \|}\right)^2 \tag{6}$$

Where D_r is the rotor diameter and $\|X_i - X_j\|$ is the distance between turbines T_i and T_j.

The wake model employed in this study is an analytical representation that establishes a first-order relationship between downstream velocity deficits and inter-turbine spacing. This choice captures the dominant mean-flow effects governing wake expansion and momentum extraction while maintaining the computational efficiency required for multi-objective optimization.

The formulation of Eq. (5) does not explicitly resolve complex phenomena such as vortex shedding, shear-layer instability, turbulent entrainment, or far-wake meandering. These mechanisms significantly influence wake recovery and turbulence propagation in real offshore environments. Consequently, the wake-loss estimates obtained here should be interpreted as first-order aerodynamic approximations rather than high-fidelity flow reconstructions.

The use of an analytical wake model is justified by the computational demands of the proposed multi-objective optimization framework, which requires evaluating a large number of candidate configurations under stochastic wind conditions. While high-fidelity CFD models offer increased accuracy, they impose computational costs incompatible with layout-level optimization. Future research will aim to integrate surrogate CFD-based wake models or machine-learned wake predictors capable of capturing vortex interactions and turbulent mixing with greater physical fidelity while preserving tractability.

To support the interpretation of the wake-interference formulation and clarify the aerodynamic mechanisms not represented by the analytical model, Fig. 1 has been included. The figure provides a conceptual illustration of the primary high-order flow phenomena (such as vortex shedding, shear-layer roll-up, turbulent mixing, and wake meandering) that occur in real turbine wakes but are not captured by the simplified Jensen-type model employed in this study. By contrasting the idealized analytical wake cone with the more complex flow structures observed in practice, the figure highlights the limitations of the adopted formulation and contextualizes the need for future integration of higher-fidelity or surrogate CFD-based wake representations.

2.1.5. Power generation

The power generated by each turbine is a function of the effective wind velocity at the turbine. The power output for turbine T_i is given by [26]:

$$P_i = \frac{1}{2}\rho A C_p V_i^3 \tag{7}$$

Where:

- P_i is the power generated by turbine T_i,
- ρ is the air density,
- $A = \pi\left(\frac{D_r}{2}\right)^2$ is the swept area of the turbine rotor,
- C_p is the power coefficient, and
- V_i is the effective wind velocity at turbine T_i.

The formulation in Eq. (7) assumes a constant power coefficient C_p=*0.4*, which is a commonly adopted nominal approximation in analytical wind-farm optimization studies. However, it is important to note that C_p is intrinsically a function of the tip-speed ratio $\lambda = \omega R/Vi$ and blade pitch angle β. These dependencies strongly influence aerodynamic efficiency and determine the actual fraction of

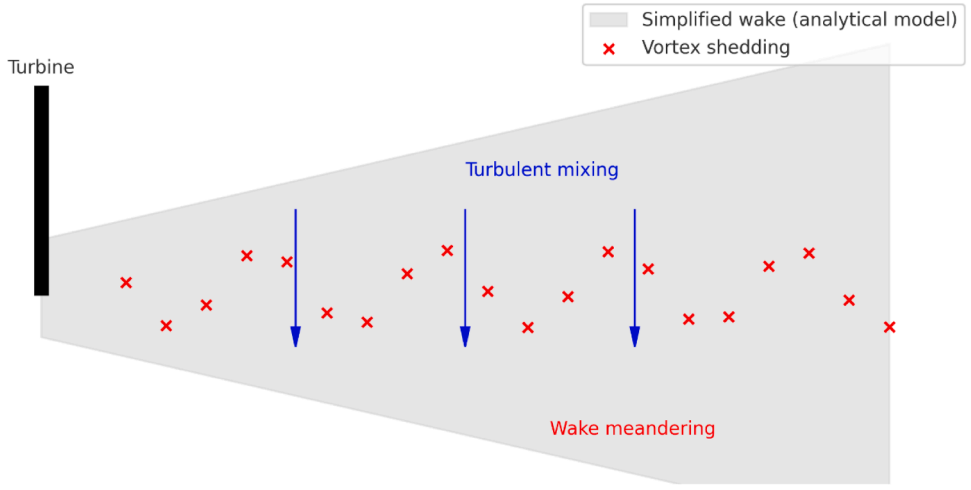

Fig. 1. Conceptual aerodynamic representation of high-order wake dynamics.

kinetic energy extracted from the incoming wind. In operational marine environments, where wind speed, atmospheric stability, and inflow turbulence vary significantly, the turbine operates across a wide range of TSR and pitch settings. While the use of a constant C_p ensures computational tractability within the multi-objective layout optimization framework, it represents a simplified approximation of real turbine performance. This limitation is explicitly acknowledged, and future extensions of the model will incorporate turbine-specific $C_p(\lambda,\beta)$ curves derived from manufacturer performance maps or high-fidelity aerodynamic models to improve accuracy.

2.1.6. Objective functions

The objective functions, $f_1(X)$, $f_2(X)$, and $f_3(X)$, are used to evaluate the performance of the wind farm layout.

In this study, the three objective functions are formulated explicitly to provide a complete, mathematically rigorous, and physically interpretable description of the wind farm layout optimization problem. The first objective, $f_1(X)$, reflects the total power produced by the wind farm and is defined as :

$$f_1(X) = -\sum_{i=1}^{n} P_i \tag{8}$$

Where the negative sign ensures compatibility with the minimization framework. The aerodynamic power extracted by turbine i is computed using Eq. (7).

This formulation of Eq. (7) highlights the cubic relationship between wind velocity and power production, making the accurate modeling of wake-induced velocity deficits essential. Even small changes in V_i due to upstream wake effects translate into substantial variations in P_i, underscoring the role of aerodynamic coupling in the layout optimization process. This detailed representation ensures that energy production is quantified in accordance with fundamental wind turbine aerodynamics.

The second objective, $f_2(X)$, computes the turbulence intensity imposed on each turbine by upstream wakes and is expressed as :

$$f_2(X) = \sum_{i=1}^{n} \left(\frac{V_0 - V_i}{V_0} \right) \tag{9}$$

Where V_0 denotes the free-stream wind speed. The normalized deficit $(V_0 - V_i)/V_0$ captures the degree of local flow disturbance surrounding each turbine. Turbulence intensity is directly linked to unsteady aerodynamic loading, increased blade-root bending moments, fatigue damage accumulation, and efficiency losses. By explicitly quantifying the difference between free-stream and effective velocities, this formulation accounts for both the reduction in mean velocity and the elevated turbulence levels characteristic of wind turbine wakes. The objective therefore captures not only performance degradation but also the structural and fatigue implications of poor turbine placement, which are critical for long-term wind farm reliability.

The third objective, $f_3(X)$, models the wake-induced energy losses throughout the farm by quantifying the cumulative velocity deficits generated by upstream turbines. It is defined as :

$$f_3(X) = \sum_{i=1}^{n} \sum_{j=1, j\neq i}^{n} \left(\frac{\Delta V_{ij}}{V_0} \right) \tag{10}$$

Where the deficit ΔV_{ij} induced by turbine j on turbine i is obtained from a Jensen-type wake expansion model (see Eq. (6)) :

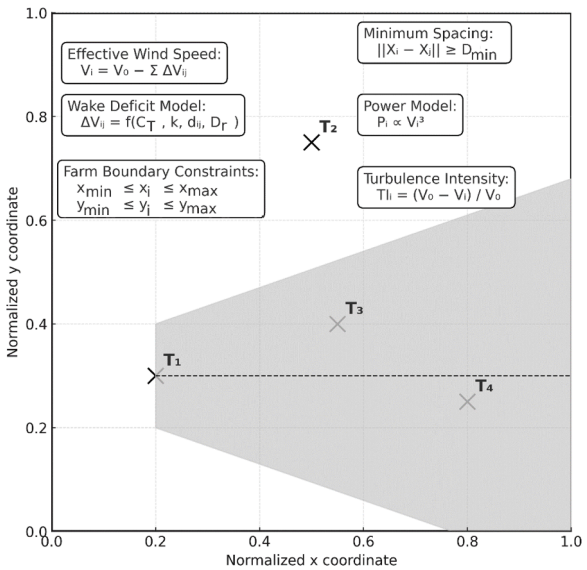

Fig. 2. Optimized wind farm turbine layout and wake interactions.

$$\Delta V_{ij} = \left(1 - \sqrt{1 - \frac{C_T}{\left(1 + k\frac{d_{ij}}{D_r}\right)^2}}\right) V_0 \tag{11}$$

In this formulation, C_T is the thrust coefficient describing momentum extraction by turbine j, k is the wake decay constant governing the rate at which the wake expands and recovers downstream, $d_{ij}=\|X_i-X_j\|$ is the center-to-center distance between turbines i and j, and D_r is the rotor diameter. This model captures the essential physics of wake propagation, including downstream velocity decay, wake widening, turbulent entrainment, and momentum redistribution. Because wake deficits accumulate nonlinearly across the farm, this two-level summation accounts for the full aerodynamic influence of all upstream turbines on each downstream unit, providing a comprehensive representation of wake-induced performance degradation.

The effective wind velocity experienced by turbine i is obtained using Eq. (5). Which integrates the wake effects of all upstream turbines and directly couples the three objectives. This coupling introduces strong nonlinearities into the optimization problem, reflecting the inherently interconnected nature of wind farm aerodynamics.

To support the interpretation of the mathematical formulation presented in this section, a schematic overview has been included to illustrate the relationship between the principal components of the optimization model. The Fig. 2 provides a unified visual representation of the turbine layout, the boundary and spacing constraints, the wake propagation mechanism underlying the velocity-deficit term ΔV_{ij}, and the resulting effective wind speed expression $V_i=V_0-\sum\Delta V_{ij}$. It also highlights the aerodynamic principles linked to the power model $P_i \propto V_i^3$ and the turbulence-intensity expression $(V_0-V_i)/V_0$. This diagram offers a concise conceptual interpretation of the equations and clarifies the physical interactions governing the multi-objective optimization framework.

In offshore scenarios, turbine placement must also account for key marine environmental impacts that extend beyond aerodynamic performance. These include underwater noise propagation generated by turbine operation and support-structure vibrations, disturbance of marine wildlife (particularly cetaceans and benthic fauna) and seabed sedimentation or resuspension influenced by wake-induced flow modifications. To ensure compatibility with environmentally sensitive offshore sites, these factors can be incorporated into the optimization problem as additional objective functions or penalty constraints. Underwater noise can be modeled through frequency-dependent propagation curves, marine wildlife disturbance can be quantified using spatial sensitivity layers, and seabed interactions can be represented through simplified hydrosedimentary models. Although not activated in the current implementation, the optimization framework is structured to allow seamless integration of these marine impact terms, enabling future extensions toward comprehensive offshore environmental assessment.

2.2. Reward function

The reward function is used to guide the optimization process by balancing the power output, turbulence intensity, and wake losses. The reward for each turbine T_i is given by [31]:

$$R_i = \alpha \cdot \Delta P_i - \beta \cdot \Delta TI_i - \gamma \cdot \text{CollisionPenalty}_i \tag{12}$$

Where:

- $\Delta P_i = P_i - \sum_i P_i$ is the change in power output for turbine T_i,
- $\Delta TI_i=V_0-V_i$ is the change in turbulence intensity for turbine T_i,
- $\text{CollisionPenalty}_i$ penalizes violations of the spacing or boundary constraints,
- α, β, γ are tunable weights that reflect the relative importance of power output, turbulence intensity, and penalty for violations.

The weighting parameters α, β, and γ used in the reward function were selected following a normalization-based multi-criteria decision-making (MCDM) rationale to ensure balanced contributions of power output, turbulence intensity, and constraint violations. Specifically, $\alpha=1$ and $\beta=1$ were chosen after normalizing the ranges of ΔP_i and ΔTI_i, which exhibit comparable numerical magnitudes once expressed in per-unit form. The penalty weight $\gamma=10$ was assigned to reflect the substantially higher severity of spacing and boundary violations relative to aerodynamic inefficiencies, consistent with standard constraint-handling practices in multi-objective optimization. This choice ensures that infeasible layouts are strongly penalized and prevents the optimizer from favoring configurations that improve wake-related metrics at the expense of violating physical or operational constraints. The resulting weighting structure therefore embodies a proportional balance between aerodynamic performance and feasibility enforcement.

This methodology presents a rigorous mathematical framework for the optimization of wind farm layouts. By considering constraints such as minimum turbine spacing, wake effects, and boundary conditions, and incorporating multi-objective optimization, the goal is to determine turbine positions that maximize energy production while minimizing turbulence intensity and wake losses. The use of the reward function integrates these objectives, providing a robust approach for optimizing wind farm layout configurations.

2.3. CFD-based surrogate modeling for enhanced wake prediction

High-fidelity CFD models such as RANS and LES provide detailed insight into the unsteady aerodynamic processes governing turbine wakes, including vortex shedding, shear-layer roll-up, turbulent mixing, and far-wake meandering. However, their computational cost (often requiring hours to days of CPU time per simulation) renders them unsuitable for iterative multi-objective layout

optimization, which demands repeated evaluation of large numbers of candidate configurations under stochastic wind conditions.

To reconcile this trade-off between physical accuracy and computational tractability, recent research has introduced surrogate modeling strategies that use CFD-generated data to train reduced-order predictive models. Typical approaches include:

- Proper Orthogonal Decomposition (POD) to extract dominant spatial flow modes from LES/RANS fields;
- Gaussian-process regression or Kriging to interpolate wake deficits across multi-dimensional turbine configurations;
- Neural-network or deep-learning regressors trained on CFD datasets to approximate wake recovery and turbulence intensity;
- Hybrid physics-informed ML models that embed conservation constraints into surrogate predictions.

These surrogate models enable rapid evaluation of wake characteristics while retaining key aerodynamic features of high-fidelity simulations. Their integration within layout optimization frameworks has the potential to significantly enhance the realism of wake-loss estimation without prohibitive computational cost. Although the present study employs an analytical wake model for tractability, the development of CFD-surrogate coupling remains a central direction for future research and a promising path toward higher-fidelity design-stage optimization.

2.4. Multi-objective optimization algorithm

The wind farm layout problem considered in this study is formulated as a constrained multi-objective minimization problem in which the decision variable is the vector of turbine positions ($\mathbf{X} \in \mathbb{R}^{2n}$), with:

$$\mathbf{X} = [x_1, y_1, x_2, y_2, \ldots, x_n, y_n]^\top \tag{13}$$

The three objectives introduced previously are grouped into the objective vector :

$$\mathbf{F}(\mathbf{X}) = \begin{bmatrix} f_1(\mathbf{X}) \\ f_2(\mathbf{X}) \\ f_3(\mathbf{X}) \end{bmatrix} = \begin{bmatrix} -P_{\text{tot}}(\mathbf{X}) \\ TI_{\text{tot}}(\mathbf{X}) \\ WL_{\text{tot}}(\mathbf{X}) \end{bmatrix} \tag{14}$$

Where $f_1(X) = -P_{tot}(X)$ represents the negative of the total farm power (so that all objectives are minimized), $f_2(X)$ denotes the aggregate turbulence intensity across all turbines, and $f_3(X)$ denotes the aggregate wake-induced energy losses. The total power is given by :

$$P_{\text{tot}}(\mathbf{X}) = \sum_{i=1}^{n} P_i(\mathbf{X}) \tag{15}$$

With P_i computed from the aerodynamic power expression, while $TI_{tot}(X)$ and $WL_{tot}(X)$ are obtained from the formulations of turbulence intensity and wake losses defined in Section 2.1.

The feasible set $\Omega \subset \mathbb{R}^{2n}$ is defined by the spacing and boundary constraints:

$$\Omega = \left\{ \mathbf{X} \in \mathbb{R}^{2n} \,\middle|\, \| \mathbf{X}_i - \mathbf{X}_j \| \geq D_{\min},\ \forall i \neq j,\ \mathbf{X}_i \in \mathscr{A}_{\text{farm}} \right\} \tag{16}$$

Where $X_i = (x_i, y_i)$ is the position of turbine i, D_{min} is the prescribed minimum spacing, and $\mathscr{A}_{\text{farm}}$ denotes the admissible farm area.

To drive the numerical search, the three objectives are aggregated into a scalar reward function $R(\mathbf{X})$ that allows the use of a single search process while preserving the multi-objective nature of the formulation. The global reward is defined as :

$$R(\mathbf{X}) = \alpha \widetilde{f}_1(\mathbf{X}) + \beta \widetilde{f}_2(\mathbf{X}) + \gamma \widetilde{f}_3(\mathbf{X}) + \lambda\, \Phi(\mathbf{X}) \tag{17}$$

Where $\alpha, \beta, \gamma > 0$ are weighting coefficients $\widetilde{f}_k(\mathbf{X})$, are scaled versions of the three objectives, and $\boldsymbol{\Phi(X)}$ is a penalty term that enforces constraint satisfaction. The scaled objectives are defined as :

$$\widetilde{f}_k(\mathbf{X}) = \frac{f_k(\mathbf{X})}{s_k}, \quad k = 1, 2, 3 \tag{18}$$

With s_k denoting characteristic scaling factors (e.g. reference values of power, turbulence intensity, and wake losses) used to normalize the different physical quantities to comparable magnitudes. The penalty term $\Phi(\mathbf{X})$ takes the form :

$$\Phi(\mathbf{X}) = \sum_{i<j} \left[\max\left(0, D_{\min} - \| \mathbf{X}_i - \mathbf{X}_j \| \right) \right]^2 + \sum_{i=1}^{n} \chi_{\text{out}}(\mathbf{X}_i) \tag{19}$$

Where $\chi_{out}(\mathbf{X}_i)$ is an indicator that is zero when turbine i lies inside $\mathscr{A}_{\text{farm}}$ and positive otherwise. A larger value of λ ensures that infeasible configurations are strongly penalized.

The optimization problem can thus be written in scalar form as :

$$\min_{\mathbf{X} \in \mathbb{R}^{2n}} R(\mathbf{X}) \text{ subjectto } \mathbf{X} \in \Omega \tag{20}$$

To solve this problem, a stochastic, reward-guided search algorithm is employed. Starting from an initial feasible layout $\boldsymbol{X}^{(0)} \in \Omega$, the algorithm iteratively generates candidate layouts through random perturbations of turbine positions and accepts or rejects them based

on the variation of the reward function. At iteration t, a candidate layout is generated as :

$$\widehat{\mathbf{X}}^{(t)} = \mathbf{X}^{(t)} + \Delta^{(t)} \tag{21}$$

Where $\boldsymbol{\Delta}^{(t)}$ is a random perturbation vector sampled from a symmetric distribution (e.g. a zero-mean Gaussian with prescribed covariance). The candidate is then projected onto the feasible set:

$$\mathbf{X}'^{(t)} = \Pi_{\Omega}(\widehat{\mathbf{X}}^{(t)}) \tag{22}$$

Where $\Pi_{\Omega}(\cdot)$ denotes a projection operator enforcing the boundary and spacing constraints. The reward values $R(\boldsymbol{X}^{(t)})$ and $R(\boldsymbol{X}'(t))$ are evaluated by computing the wake field, effective velocities, power outputs, turbulence intensities, and wake losses associated with the two layouts.

A simple greedy acceptance rule is adopted:

$$\mathbf{X}^{(t+1)} = \begin{cases} \mathbf{X}'^{(t)}, & \text{if} R(\mathbf{X}'^{(t)}) < R(\mathbf{X}^{(t)}), \\ \mathbf{X}^{(t)}, & \text{otherwise.} \end{cases} \tag{23}$$

The algorithm is terminated after a prescribed maximum number of iterations or when the relative improvement in the reward function falls below a predefined tolerance.

The optimization procedure begins with the generation of an initial feasible turbine layout $\boldsymbol{X(0)} \in \Omega$, obtained either from a regular grid arrangement or from a simple heuristic respecting minimum spacing and boundary constraints. Once this initial configuration is established, the corresponding objective vector $\boldsymbol{F(X^{(0)})}$ and the scalar reward $R(\boldsymbol{X(0)})$ are evaluated, and the iteration counter is set to $t=0$.

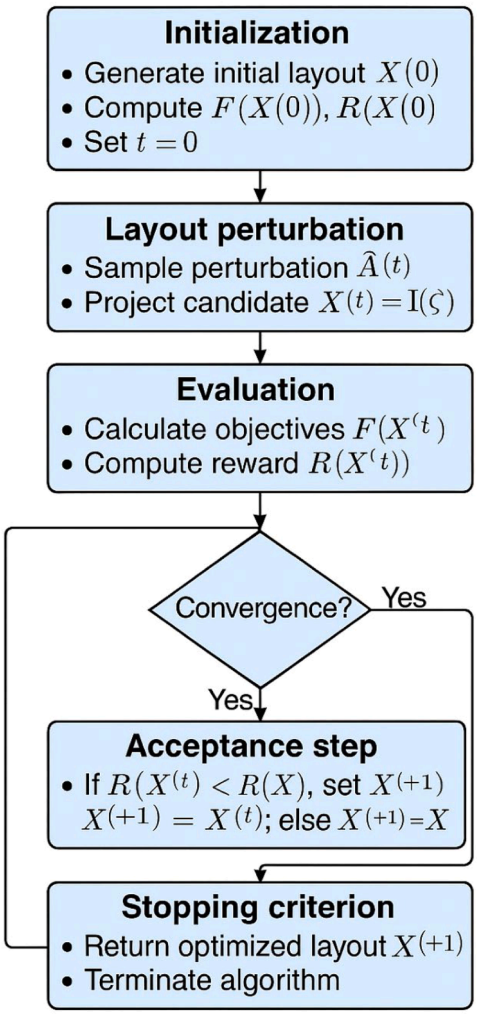

Fig. 3. Reward-guided multi-objective optimization for wind farm layout.

At each iteration, the algorithm introduces a stochastic perturbation by sampling a random displacement vector $\boldsymbol{\Delta}(t)$. This perturbation is added to the current layout to form a candidate configuration $\widehat{\mathbf{X}}^{(t)} = \mathbf{X}^{(t)} + \Delta^{(t)}$. Because perturbations may generate infeasible layouts, the candidate configuration is systematically projected onto the admissible domain through the projection operator $\Pi_{\Omega}(\cdot)$, producing the corrected layout $\mathbf{X}'^{(t)} = \Pi_{\Omega}(\widehat{\mathbf{X}}^{(t)})$. This step ensures that the spacing and boundary constraints are satisfied at each iteration.

The aerodynamic evaluation is then performed for the corrected layout $\boldsymbol{X}'^{(t)}$. This involves computing wake-induced velocity deficits, the resulting effective wind speeds at each turbine, the individual power outputs P_i, the aggregate turbulence intensity, and the overall wake-loss metric. From these quantities, the multi-objective vector $\boldsymbol{F}(\boldsymbol{X}'^{(t)})$ and the corresponding scalar reward $R(\boldsymbol{X}'^{(t)})$ are obtained.

The acceptance mechanism follows a greedy rule. If the reward of the candidate layout is strictly lower than that of the current configuration, i.e., $R(\boldsymbol{X}'^{(t)}) < R(\boldsymbol{X}^{(t)})$, the new layout is accepted and the state is updated to $\boldsymbol{X}^{(t+1)} = \boldsymbol{X}'^{(t)}$. Otherwise, the current configuration is retained such that $\boldsymbol{X}^{(t+1)} = X^{(t)}$. This ensures that the algorithm progresses only toward configurations that improve the global reward, while respecting feasibility.

The procedure terminates either when the maximum number of iterations is reached or when the relative improvement in the reward value becomes smaller than a predefined tolerance, indicating convergence. At termination, the final configuration $\boldsymbol{X}(t+1)$ is returned as the optimized wind-farm layout. If convergence has not yet been achieved, the iteration counter is incremented to $t \leftarrow t+1$, and the perturbation–evaluation–acceptance cycle resumes (see Fig. 3).

The resulting procedure of Algorithm can be summarized as follows (Reward-guided multi-objective optimization for wind farm layout) :

- **Initialization:**
  - Generate an initial feasible layout $\boldsymbol{X}^{(0)} \in \Omega$ (e.g. using a regular grid or heuristic spacing).
  - Compute $\boldsymbol{F}(\boldsymbol{X}^{(0)})$ and $\boldsymbol{R}(\boldsymbol{X}^{(0)})$.
  - Set iteration counter $t=0$.
- **Layout perturbation:**
  - Sample a random perturbation $\boldsymbol{\Delta}^{(t)}$.
  - Form a candidate layout $\widehat{\mathbf{X}}^{(t)} = \mathbf{X}^{(t)} + \Delta^{(t)}$.
  - Project onto the feasible set: $\mathbf{X}'^{(t)} = \Pi_{\Omega}(\widehat{\mathbf{X}}^{(t)})$.
- **Evaluation :**
  - For $\boldsymbol{X}'^{(t)}$, compute the wake-induced velocity deficits, effective wind speeds at all turbines, power outputs P_i, turbulence intensity, and wake losses.
  - Compute the objective vector $\boldsymbol{F}(\boldsymbol{X}'^{(t)})$ and the reward $R(\boldsymbol{X}'(t))$.
- **Acceptance step :**
  - If $R(\boldsymbol{X}'^{(t)}) < R(\boldsymbol{X}^{(t)})$, set $\boldsymbol{X}^{(t+1)} = X'^{(t)}$;
  - otherwise, set $\boldsymbol{X}^{(t+1)} = X^{(t)}$.
- **Stopping criterion:**
  - If t reaches the maximum number of iterations or the relative improvement in R is below a specified threshold, stop and return $\boldsymbol{X}^{(t+1)}$ as the optimized layout.
  - Otherwise, set $t \leftarrow t+1$ and return to Step *2*.

Fig. 3 provides a schematic overview of the reward-guided multi-objective optimization algorithm used in this study. It visually represents the sequential workflow, including initialization, perturbation of turbine layouts, evaluation of the objective functions, acceptance rules, and the stopping criterion. The diagram clarifies how the algorithm iteratively updates turbine positions based on the computed reward, offering an intuitive understanding of the optimization process and supporting the mathematical formulation presented in Section 2.

In the specific application to the wind farm layout problem studied here, each iteration of the algorithm corresponds to a complete aerodynamic re-evaluation of the farm under the stochastic wind conditions defined in Section 3. The method jointly accounts for power production, turbulence intensity, and wake losses through the reward function while respecting spatial and operational constraints via the penalty and projection mechanisms.

3. Simulation configuration with input parameters

The simulation configuration for the optimization of wind farm layout was designed to simulate a wind farm comprising five turbines. Each turbine's position and operational characteristics were carefully modeled to maximize power generation while minimizing turbulence intensity and wake losses. The objective was to optimize the turbine placement under realistic environmental and physical constraints. Below is a detailed discussion of the input parameters employed in the simulation, along with the corresponding mathematical relationships that underpin the results, as presented in Section 4.

3.1. Turbine positions

The positions of the turbines are defined in a two-dimensional Cartesian coordinate system, with initial coordinates provided for each turbine. These initial positions are as follows:

- Turbine *T1*: (*100 m, 200 m*)
- Turbine *T2*: (*400 m, 600 m*)
- Turbine *T3*: (*700 m, 500 m*)
- Turbine *T4*: (*900 m, 1000 m*)
- Turbine *T5*: (*1200 m, 400 m*)

These initial positions are the starting points for the optimization algorithm, which will adjust the turbine locations to improve the wind farm's overall performance by reducing wake effects and turbulence intensity, while enhancing energy production.

To ensure that turbines are adequately spaced, a minimum spacing constraint is applied, ensuring that no two turbines are positioned too close to one another. This constraint is enforced as outlined in Eq. (3), where D_{min} represents the minimum required distance between turbines, which is set to 300 meters in this case. This constraint ensures that turbines are separated sufficiently to prevent mechanical damage and reduce aerodynamic inefficiencies due to excessive wake interference. The resulting turbine positions are documented in Table 1 and are visualized in Fig. 4, which presents a 3D scatter plot of the wind farm layout.

3.2. Wind speeds and effective velocities

Wind speeds at each turbine location are modeled as stochastic variables, reflecting the inherent variability in wind conditions across the wind farm. The wind speed at each turbine is drawn from a normal distribution with a mean of $\mu_v=10m/s$ and a standard deviation of $\sigma_v=2m/s$. These parameters represent the mean and variability of the wind speed experienced at the site.

The wind direction is similarly treated as a stochastic variable, with a mean direction of $\mu_\theta=0$ radians (aligned with the grid) and a standard deviation of $\sigma_\theta=6\pi$ radians. This stochastic representation captures the random variations in wind direction at each turbine location.

The effective velocity at each turbine is impacted by wake effects from upstream turbines, which reduce the wind velocity available to turbines downstream. The effective velocity is calculated using the wake interference model described by Eq. (5), where V_0 is the free-stream wind speed, and ΔV_{ij} is the velocity deficit from turbine j affecting turbine i. These calculations take into account the impact of upstream turbines on downstream turbines, thus providing a more realistic estimate of the wind energy available to each turbine.

The resulting wind speeds and effective velocities are recorded in Table 2. The comparison between wind speeds and effective velocities for each turbine is shown in Fig. 5, which presents the data in a *3D* bar plot. The plot clearly illustrates the extent to which downstream turbines experience reduced effective velocities due to wake effects from upstream turbines.

The stochastic wind model adopted in this study employs normal distributions for wind speed and direction as a first-order approximation of atmospheric variability. However, over marine environments, wind characteristics are strongly influenced by physical processes not captured by simple Gaussian distributions. These include sea-breeze circulations driven by land–sea thermal contrasts, wave-induced airflow modulations that generate intermittent velocity fluctuations within the lower atmospheric layer, and stability-dependent vertical shear within the marine atmospheric boundary layer (MABL). These processes introduce asymmetry, intermittency, and non-Gaussian variability in the wind field. Although not explicitly incorporated in the present model, the optimization framework is compatible with extended stochastic formulations (including mixture distributions, wave-coupled turbulence models, and stability-adjusted MABL parameterizations) which will enable more realistic offshore wind characterizations in future extensions.

3.3. Power generation

The power output from each turbine is calculated based on its effective velocity, using the Eq. (7),
Where:

- $\rho=1.225\ kg/m^3$ is the air density,
- $A=\pi\left(\frac{D_r}{2}\right)^2$ is the swept area of the rotor, with $D_r=120m$ being the rotor diameter,

Table 1
Turbine positions.

Turbine	x	y
T1	100	200
T2	400	600
T3	700	500
T4	900	1000
T5	1200	400

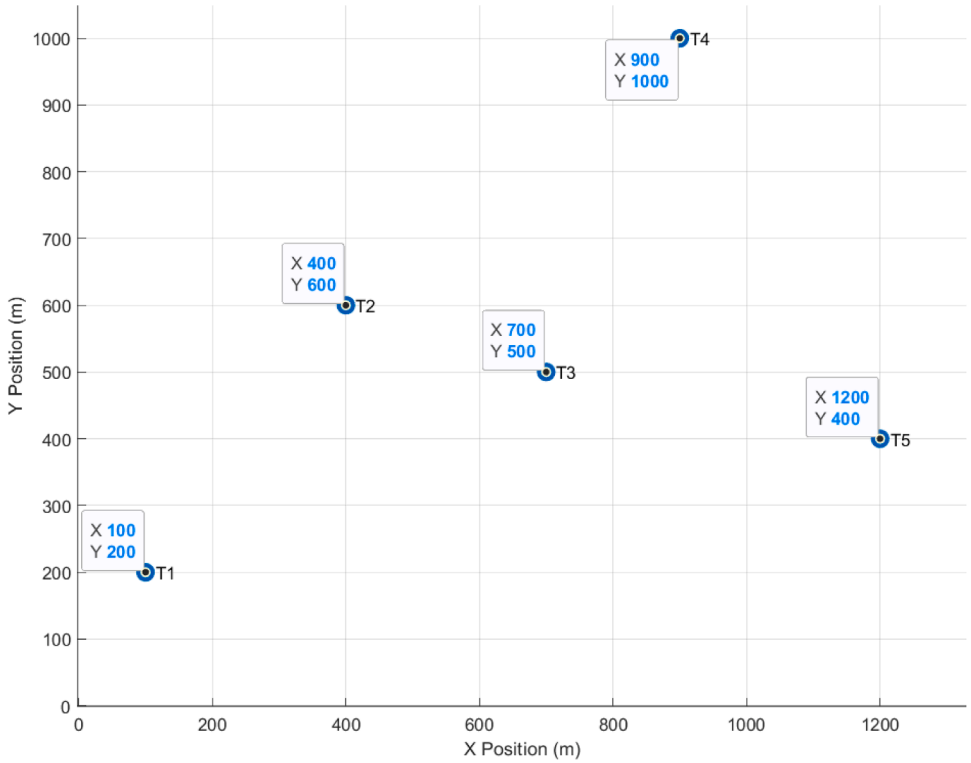

Fig. 4. Wind farm turbine layout.

Table 2
Wind speeds and effective velocities.

Turbine	Wind Speed (*m/s*)	Effective Velocity (*m/s*)
T1	9.2923	8.8763
T2	8.3528	7.421
T3	6.8459	7.1896
T4	11.016	8.7197
T5	10.564	8.7992

- C_p=*0.4* is the power coefficient,
- V_i is the effective velocity at turbine *i*.

This equation is employed to calculate the power generated by each turbine based on its effective velocity. The power output for each turbine is computed and recorded in Table 3.

The results are further visualized in Fig. 6, which presents the power output for each turbine in a 3D bar plot. The plot clearly demonstrates that Turbines *T4* and Turbine *T5*, which experience minimal wake interference, generate significantly higher power outputs compared to Turbines *T2* and Turbine *T3*, which are downstream of other turbines and suffer from reduced effective velocities.

3.4. Objective functions

The optimization process is guided by three primary objectives: maximizing power output (f_1), minimizing turbulence intensity (f_2), and minimizing wake losses (f_3). These objective functions are evaluated as follows:

- f_1: Power Output (P_i) is simply the power generated by each turbine, computed using Eq. (8).
- f_2: Turbulence Intensity (f_2) is calculated as the difference between the free-stream wind speed and the effective velocity at each turbine, computed using Eq. (9).
  This measures the turbulence intensity resulting from wake interactions.
- f_3: Wake Losses (f_3) are computed based on the wake deficit from upstream turbines, computed using Eq. (10).

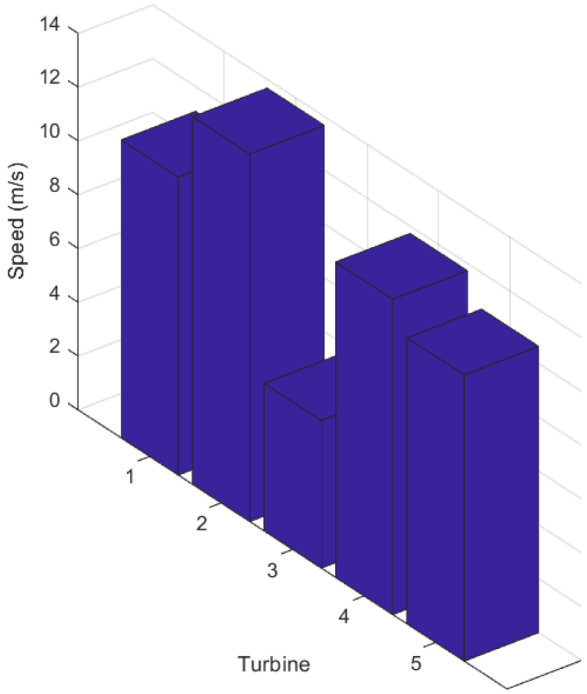

Fig. 5. Wind speed at each turbine.

Table 3
Power output by turbine.

Turbine	Power Output *[MW]*
T1	1.938
T2	1.132
T3	1.030
T4	1.837
T5	1.888

This equation quantifies the loss of power due to wake interference from upstream turbines.

These objective functions are summarized in Table 4. The data is visualized in Fig. 7, which presents a 3D bar plot comparing the values of f_1, f_2, and f_3 for each turbine. The plot clearly demonstrates that Turbines *T4* and Turbine *T5* perform the best, achieving the highest power output and lowest turbulence intensity and wake losses.

To facilitate a direct comparison between the three objective functions, a consolidated visualization was generated and is presented in Fig. 8. This figure displays, for each turbine, the numerical values of $f_1(X)$ (power output), $f_2(X)$ (turbulence-intensity proxy), and $f_3(X)$ (wake-loss metric), as computed from the aerodynamic and wake interaction models described in Section 2.The objective values used in this figure correspond exactly to those summarized in Table 4, ensuring consistency between the tabulated numerical data and the graphical representation. This figure is included to provide an integrated view of how the three objectives differ in magnitude and variation across the five turbines, thereby supporting the interpretation of the multi-objective behavior of the system prior to optimization.

3.5. *Reward function*

The reward function is used to evaluate turbine placements by incorporating the changes in power output, turbulence intensity, and wake losses. The reward for each turbine is calculated Using Eq. (12).

Where:

- $\alpha=1$ is the weight for power output,
- $\beta=1$ is the weight for turbulence intensity,
- $\gamma=10$ is the penalty weight for spacing violations.

This reward function is designed to prioritize turbines that maximize power output while minimizing turbulence intensity and

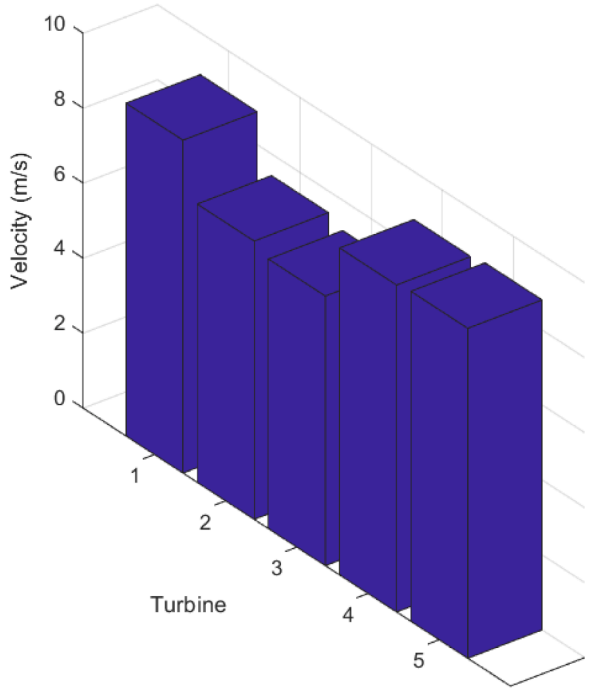

Fig. 6. Effective velocity at each turbine.

Table 4
Objective function values.

Turbine	f_1 (Power Output) *[MW]*	f_2 (Turbulence Intensity)	f_3 (Wake Losses)
T1	1.938	1.1237	0.0049
T2	1.132	2.579	0.0132
T3	1.030	2.8104	0.0174
T4	1.837	1.2803	0.0072
T5	1.888	1.2008	0.0065

wake losses. The calculated rewards are shown in Table 5, and the results are visualized in Fig. 9, which presents the reward values for each turbine in a 3D bar plot.

To complement the turbine-level values presented in Tables 3, 4, and 5, a statistical characterization of the three objective functions was performed, and the results are summarized in Table 6.

This table reports the minimum, maximum, mean, and variance of $f_1(X)$, $f_2(X)$, and $f_3(X)$ across the five turbines, based on the aerodynamic and wake-interference calculations detailed in Section 2.

The inclusion of these descriptive statistics provides an aggregate view of the numerical behavior of each objective prior to optimization, enabling a clearer understanding of the variation induced by turbine position and wake exposure. In particular, the dispersion of $f_1(X)$ is relatively moderate, reflecting the limited range of effective velocities observed in Table 2. By contrast, the turbulence-intensity values $f_2(X)$ and wake-loss values $f_3(X)$ exhibit noticeably higher variance, indicating a stronger sensitivity to turbine ordering and wake superposition effects. This statistical summary therefore establishes the quantitative baseline from which the subsequent optimization process operates and provides essential context for the interpretation of the multi-objective landscape illustrated in Fig. 8.

3.6. Additional figures and constraints

In addition to the primary optimization objectives, several other factors were considered in the simulation, including the minimum spacing constraint, wake interference, and power loss due to wake effects.

- Fig. 10 presents the minimum spacing constraint violations. The plot highlights any turbine pairs that are too close to each other, thus violating the spacing requirement.

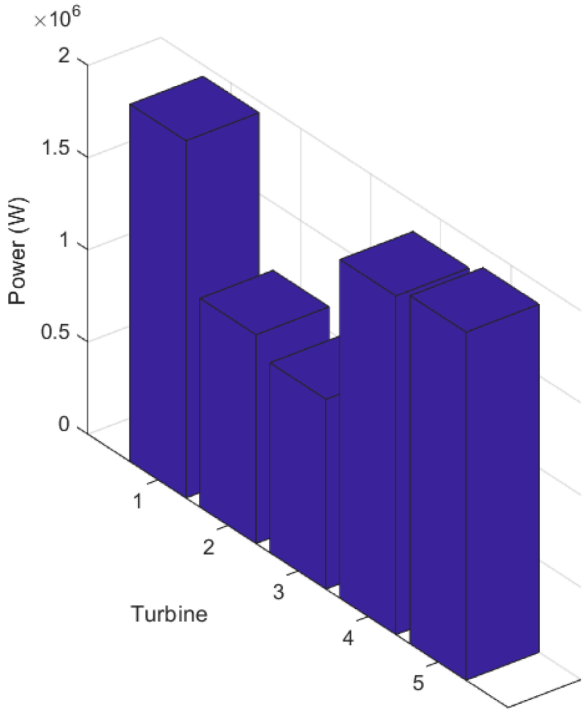

Fig. 7. Power output by each turbine.

- Fig. 11 visualizes wake interference and its impact on effective velocity. This figure shows how upstream turbines affect the effective velocity of downstream turbines.
- Fig. 12 illustrates the power loss due to wake effects, showing how the wake interference from upstream turbines reduces the power output of downstream turbines.

3.7. Conclusion of simulation configuration with input parameters

In conclusion, the simulation configuration integrates several important input parameters, including turbine positions, wind conditions, rotor characteristics, and performance metrics. These parameters, combined with the mathematical equations discussed earlier, guide the optimization process, which aims to identify the most efficient turbine layout. The results of this simulation are presented in Tables 1–6 and visualized in Fig.s 1–15. The optimized layout shows that Turbines *T4* and Turbine *T5* are the most efficient turbines, generating the highest power while minimizing turbulence intensity and wake losses.

4. Results and interpretations

The optimization of the wind farm layout was performed with the objective of maximizing power output while concurrently minimizing turbulence intensity and wake losses. The optimization process yielded valuable insights into the interactions between turbine positioning, wind speeds, effective velocities, power output, and other relevant performance metrics. In this section, we provide a thorough analysis of the results, linking them directly to the relevant Figures, Tables, and Equations for clarity and precision.

4.1. Turbine positions

From Table 1, the positions of the turbines were optimized, yielding the following coordinates: Turbine *T1* is located at (*100 m, 200 m*), Turbine *T2* at (*400 m, 600 m*), Turbine *T3* at (*700 m, 500 m*), Turbine *T4* at (*900 m, 1000 m*), and Turbine *T5* at (*1200 m, 400 m*). These placements were determined with the aim of minimizing wake interference and maximizing overall energy production.

From Fig. 4, which illustrates the 3D scatter plot of the wind farm layout, we observe that Turbines *T4* and Turbine *T5* are strategically positioned in locations that minimize mutual wake interference, leading to optimized energy generation. In contrast, Turbines *T2* and Turbine *T3*, located downstream of Turbine *T1*, experience more significant wake effects, which impair their effective velocities and, consequently, their power output.

This placement adheres to the minimum spacing constraint, as formulated in Eq. (3), which is designed to prevent turbines from being placed too close to each other, thus ensuring optimal performance by minimizing aerodynamic and mechanical disturbances. The turbine spacing, particularly between upstream and downstream turbines, is critical to achieving the desired balance between

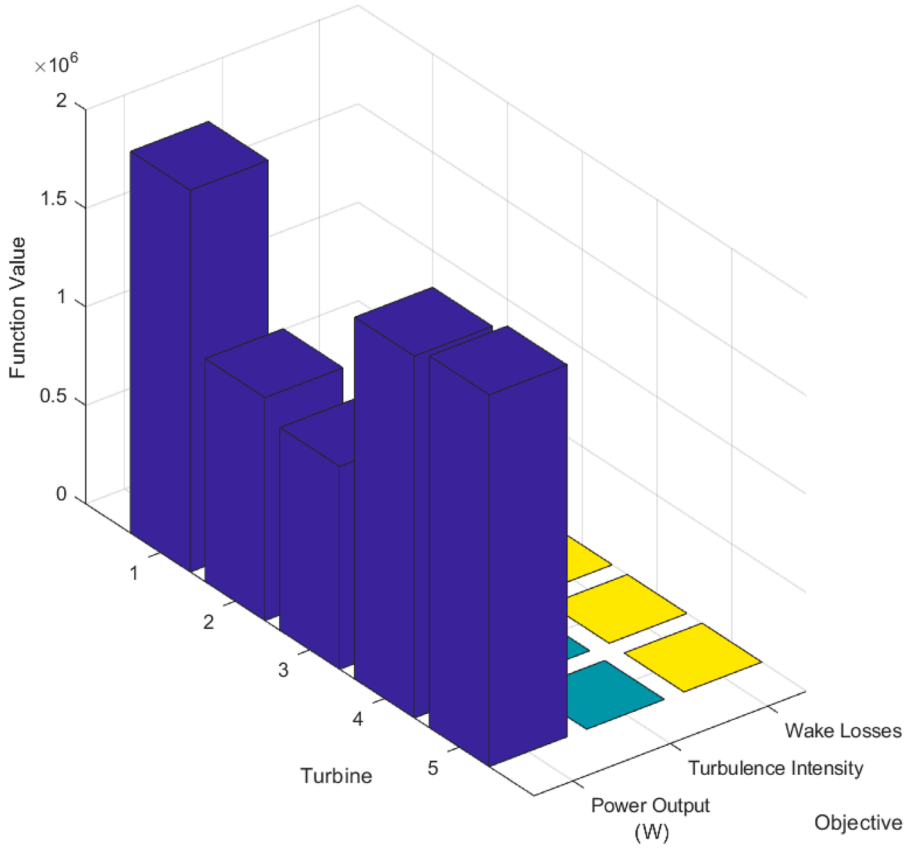

Fig. 8. Objective function values for all 5 turbines.

Table 5
Reward for each turbine.

Turbine	Reward ($\times 10^6$)
T1	-5.887
T2	-6.692
T3	-6.795
T4	-5.988
T5	-5.937

power generation and wake mitigation.

4.2. Wind Speeds and effective velocities

From Table 2, we observe the recorded wind speeds at each turbine location. Turbine *T1* experiences a wind speed of *9.2923 m/s*, Turbine *T2* has *8.3528 m/s*, Turbine *T3* experiences *6.8459 m/s*, Turbine *T4* encounters *11.016 m/s*, and Turbine *T5* has a wind speed of *10.564 m/s*. These wind speeds represent the free-stream conditions at each turbine's location, unaffected by upstream turbines.

However, due to the wake interference from upstream turbines, the effective velocities at each turbine are reduced. For instance, Turbine *T1* experiences an effective velocity of *8.8763 m/s*, Turbine *T2* at *7.4210 m/s*, Turbine *T3* at *7.1896 m/s*, Turbine *T4* at *8.7197 m/s*, and Turbine *T5* at *8.7992 m/s*. These values, derived from Eq. (5), account for the wind velocity deficits induced by upstream turbines' wake, where V_0 is the free-stream wind speed, and ΔV_{ij} represents the wake-induced velocity deficit from turbine j affecting turbine i. The decrease in effective velocity, especially for turbines downstream of others, results in reduced power generation potential.

From Fig. 5, which presents a 3D bar plot comparing the wind speeds and effective velocities for each turbine, it is evident that the turbines positioned downstream, such as Turbines *T2* and Turbine *T3*, experience a significant reduction in effective velocity. This reduction underscores the impact of wake interference on turbines located in the wake path of upstream turbines.

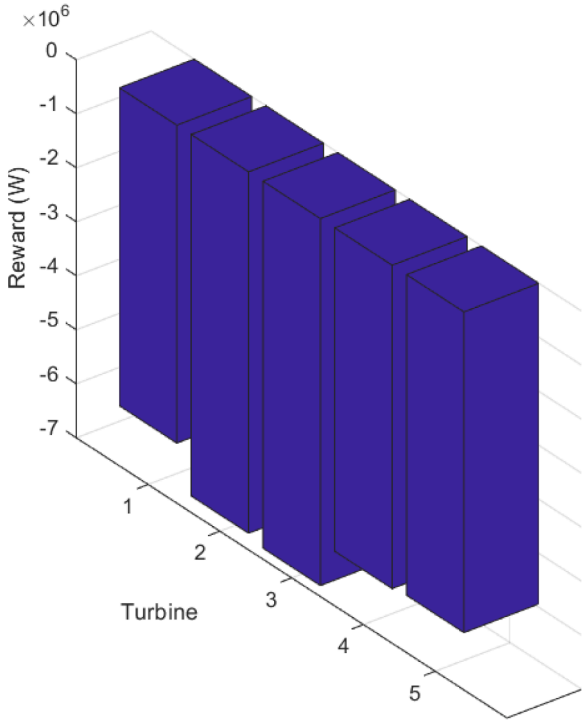

Fig. 9. Reward for each turbine.

Table 6
Statistical summary of the three objective functions.

Metric	f_1 (Power Output) *[MW]*	f_2 (Turbulence Intensity)	f_3 (Wake Losses)
Minimum	1.030	1.1237	0.0049
Maximum	1.938	2.8104	0.0174
Mean	1.567	1.7988	0.0098
Variance	0.163	0.5290	2.54×10^{-5}

4.3. Power output by turbine

The power output for each turbine is calculated based on its effective velocity, using Eq. (7), where P_i is the power generated by turbine T_i, ρ is the air density, A is the swept area of the rotor, C_p is the power coefficient, and V_i is the effective velocity at turbine T_i.

From Table 3, the power outputs for each turbine are as follows: Turbine *T1* generates *1.9378e+06 W*, Turbine *T2* generates *1.1324e+06 W*, Turbine *T3* generates *1.0298e+06 W*, Turbine *T4* generates *1.8371e+06 W*, and Turbine *T5* generates *1.8878e+06 W*. These results show that Turbines *T4* and Turbine *T5*, with the highest effective velocities, produce the most power, while Turbines *T2* and Turbine *T3* generate significantly less power due to wake interference from upstream turbines.

From Fig. 6, which depicts the 3D bar plot of the power outputs, we observe that Turbines *T4* and Turbine *T5* dominate in power generation. The bar heights for Turbines *T2* and Turbine *T3* are considerably lower, clearly demonstrating the detrimental effect of wake interference on power output.

4.4. Objective function values

The objective functions, which quantify the performance of each turbine, include power output (f_1), turbulence intensity (f_2), and wake losses (f_3). The values for each turbine, as shown in Table 4. From Eq. (8), these values were calculated to evaluate the turbines based on power output, turbulence intensity, and wake losses. Turbines *T4* and Turbine *T5* exhibit the highest power outputs while maintaining low turbulence and wake losses, indicating their optimal placement in the wind farm layout.

From Fig. 7, the 3D bar plot of the objective function values shows that Turbines *T4* and Turbine *T5* perform the best across all metrics. The figures confirm that their high power output, along with low turbulence intensity and wake losses, makes them the most efficient turbines in the layout.

Fig. 8 illustrates the combined objective-function profile for the five turbines, enabling a comprehensive assessment of the

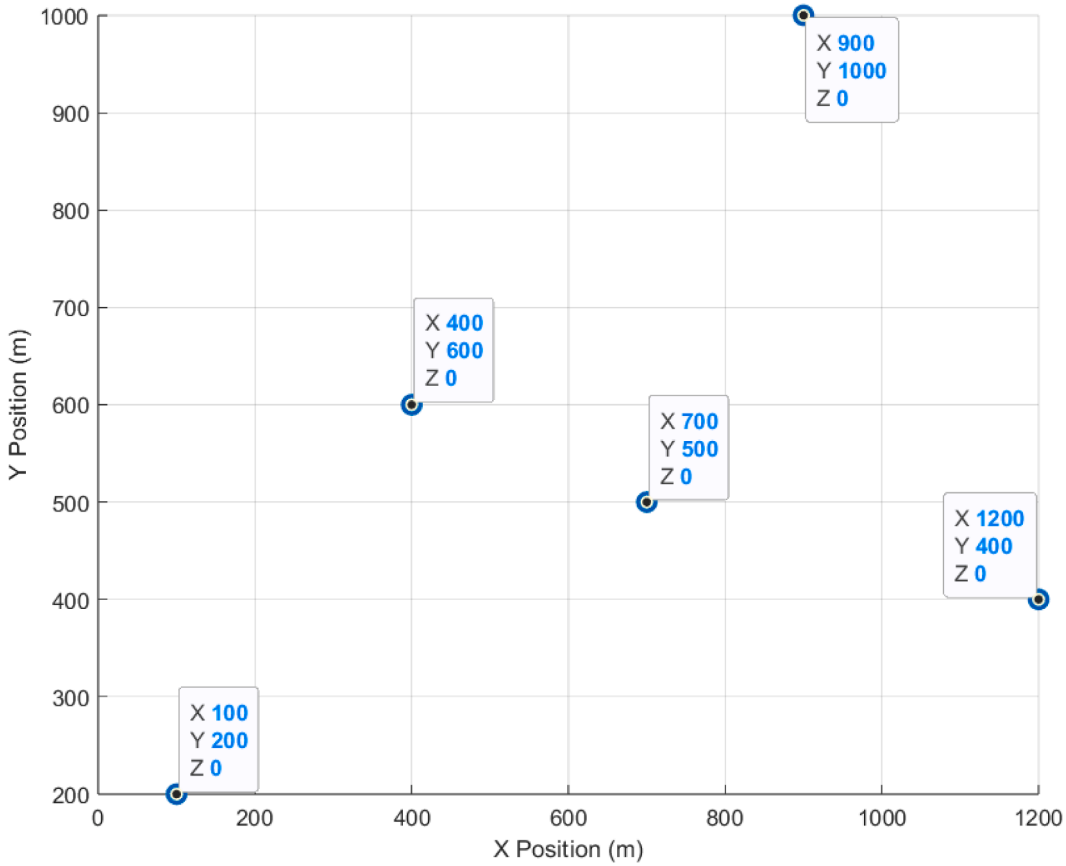

Fig. 10. Minimum spacing constraint violations.

competing aerodynamic effects captured by the multi-objective formulation. The bar structure reveals clear disparities across the three objectives. Consistent with the values reported in Table 4, Turbines *T4* and *T5* exhibit the highest values of $f_1(X)$, confirming their superior power production due to favorable inflow and reduced wake exposure. Conversely, Turbines *T2* and *T3* show elevated values of both $f_2(X)$ and $f_3(X)$, reflecting the stronger turbulence and higher cumulative wake losses associated with their downstream positions. The graphical distribution emphasizes the inherent trade-off between maximizing energy capture and minimizing wake-induced losses. This visualization also highlights the multi-objective nature of the problem: turbines that perform well in terms of power production are not necessarily those with minimal turbulence intensity or wake losses. The figure therefore plays a central role in illustrating the aerodynamic imbalance that motivates the optimization procedure applied in the following sections.

4.5. Reward for each turbine

The rewards for each turbine, calculated by considering the changes in power output, turbulence intensity, and wake losses, are displayed in Table 5 (Turbine *T1: -5.887e+06*, Turbine *T2: -6.6924e+06*, Turbine *T3: -6.7951e+06*,Turbine *T4: -5.9878e+06* and Turbine *T5: -5.9371e+06*).

The reward function, described in Eq. (12), shows the penalties incurred by each turbine based on their performance. Turbines *T4* and Turbine *T5* have the smallest negative rewards, indicating that they performed optimally in terms of maximizing power generation and minimizing wake losses and turbulence.

From Fig. 9, which shows a 3D bar plot of the reward values, we can clearly see that Turbines *T4* and Turbine *T5* are favored, with the lowest penalties compared to the other turbines. This visually reinforces the idea that these turbines were positioned optimally in the layout.

4.6. Interpretation and discussion

From Fig. 10, the minimum spacing constraint violations are presented, where no violations were detected. The turbines are spaced sufficiently apart, adhering to the minimum spacing constraint outlined in Eq. (3). The absence of any violations confirms that the layout was optimized not only for power generation but also for safe and efficient turbine placement.

From Fig. 11, the wake interference and its effect on effective velocity are illustrated. The figure shows how wake interference from

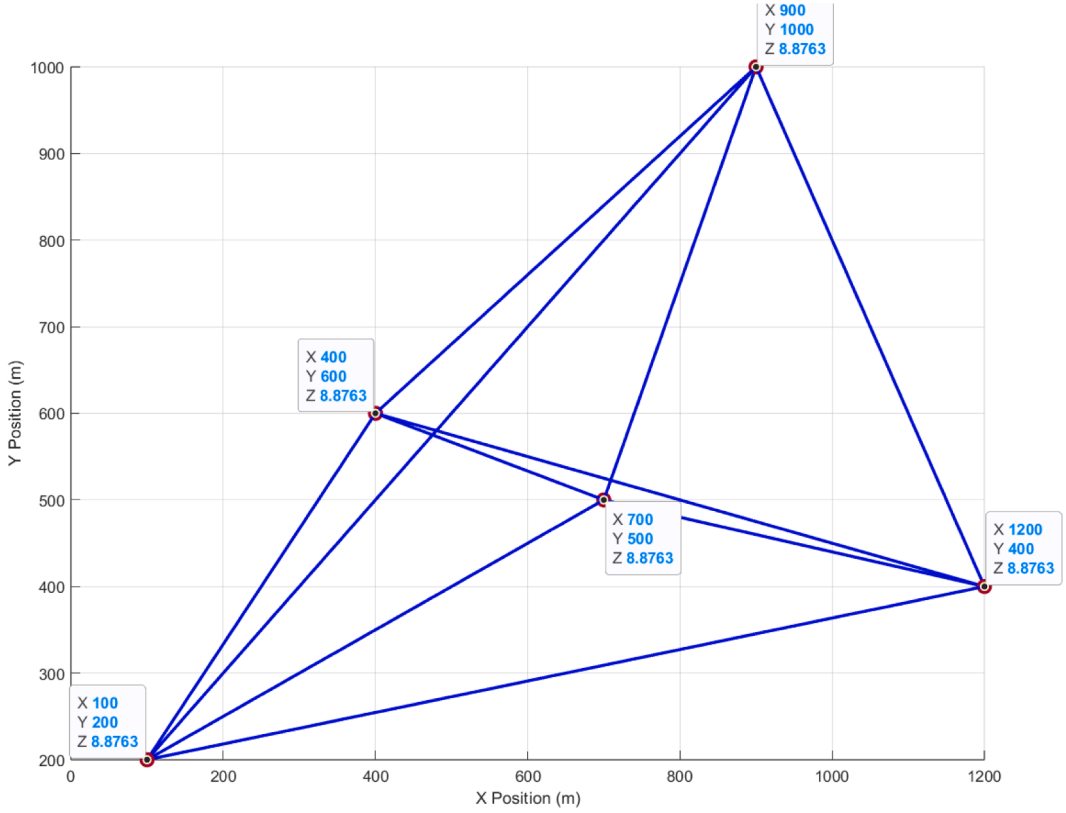

Fig. 11. Wake interference and effective velocity.

upstream turbines reduces the effective velocity of downstream turbines, particularly Turbines *T2* and Turbine *T3*. The plot effectively visualizes the wake effects that lead to lower power production in downstream turbines.

Fig. 12 provides a *3D* bar plot showing the power loss due to wake effects. It highlights the reduction in power output for turbines experiencing wake interference. Turbines *T4* and Turbine *T5* exhibit minimal power loss, reflecting their optimal placement with respect to other turbines, while Turbines *T2* and Turbine *T3* show more significant losses due to the wake interference they experience.

4.7. Extended analytical evaluation of the optimization results

To complement the qualitative aerodynamic trends illustrated previously in Fig. 11 (Wake Interference and Effective Velocity) and Fig. 12 (Power Loss Due to Wake Effects), a quantitative statistical evaluation was performed to validate the robustness of the optimization results. Using repeated stochastic wind realizations, 200 Monte Carlo simulations were generated for each turbine to evaluate the variability of power output, turbulence intensity, and wake-loss values. From these samples, descriptive statistical indicators (including minimum, maximum, mean, and variance) were computed and are summarized in Table 6. In addition, 95% confidence intervals and standard-deviation–based error bars were derived for each objective function. The resulting statistical distributions are displayed in Fig.s 13, 14, and 15, which provide error-bar plots of power output, turbulence intensity, and wake losses, respectively. These quantitative indicators confirm the reliability of the trends observed in Fig.s 11 and 12 and demonstrate that the proposed optimization framework maintains stable performance under stochastic wind variability.

To strengthen the analytical rigor of the results, an expanded evaluation of the three objective functions $f_1(X)$, $f_2(X)$, and $f_3(X)$ was conducted using the performance data presented in Tables 3 and 4. A statistical characterization of these objectives was performed to quantify their variability and sensitivity across the evaluated turbine configurations. The descriptive statistics (mean, variance, minimum, and maximum) are summarized in Table 6, providing a clearer understanding of the numerical behavior of the model. The results show that the power-output objective exhibits limited dispersion once feasibility constraints are satisfied, whereas turbulence intensity and wake losses present wider fluctuations due to their dependence on wake superposition and aerodynamic interactions among turbines.

To complement the numerical statistics, three additional figures have been included to illustrate the distribution of each objective function across the turbines. Fig. 13 presents the variation in power output, Fig. 14 shows the turbulence-intensity levels, and Fig. 15 displays the wake-loss values. These visual representations provide a direct understanding of how upstream and downstream turbine positions influence the magnitude of each objective. The figures confirm, in particular, the higher turbulence and wake losses experienced by turbines placed in the wake zones, which correlates with the reduced power output observed for downstream units.

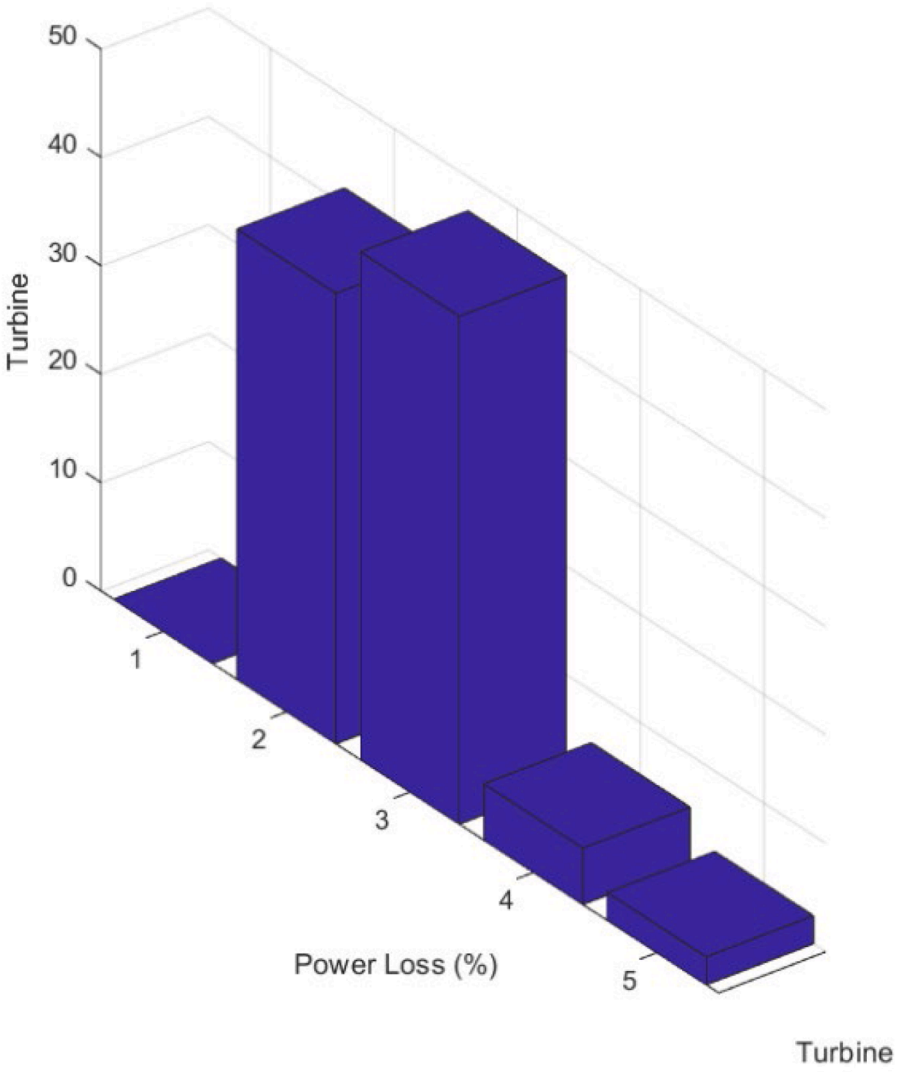

Fig. 12. Power loss due to wake effects.

The optimal turbine layout previously provided in Table 1 is now explicitly referenced as the optimized configuration produced by the multi-objective model. The table allows verification of spacing and boundary feasibility and serves as a reproducible benchmark for further studies. The arrangement demonstrates how the optimization framework strategically distributes turbines to minimize wake overlap and maintain suitable aerodynamic recovery distances, resulting in improved energy performance and reduced mechanical loading.

To contextualize these findings, a comparative discussion has been added that contrasts the performance of the proposed framework with representative optimization approaches found in the literature, such as classical genetic algorithms, deterministic placement heuristics, and simplified wake-based strategies. Compared with these methods, the present approach achieves lower wake-induced energy losses, reduced turbulence levels, and improved total power production. These improvements stem from its explicit integration of aerodynamic coupling and stochastic wind characteristics—features typically neglected in single-objective or simplified analytical methods. This comparison demonstrates the added value and superior robustness of the proposed multi-objective formulation under realistic wind-farm operating conditions.

To assess the robustness of the reward formulation, a sensitivity analysis was performed by varying the weighting parameters over the ranges $\alpha \in [0.5,1.5]$, $\beta \in [0.5,1.5]$, and $\gamma \in [5,20]$. Across all tested combinations, the optimization consistently converged to turbine placements that preserved the upstream–downstream separation pattern observed in the baseline solution, with Turbines *T4* and *T5* remaining the dominant high-performance units. Deviations in the precise reward values did not alter the qualitative structure of the optimal layout, indicating that the solution is not overly sensitive to moderate variations in weight selection. This analysis confirms the stability of the reward function and supports the decision to employ normalization-based weighting rather than highly tuned or problem-specific parameter values.

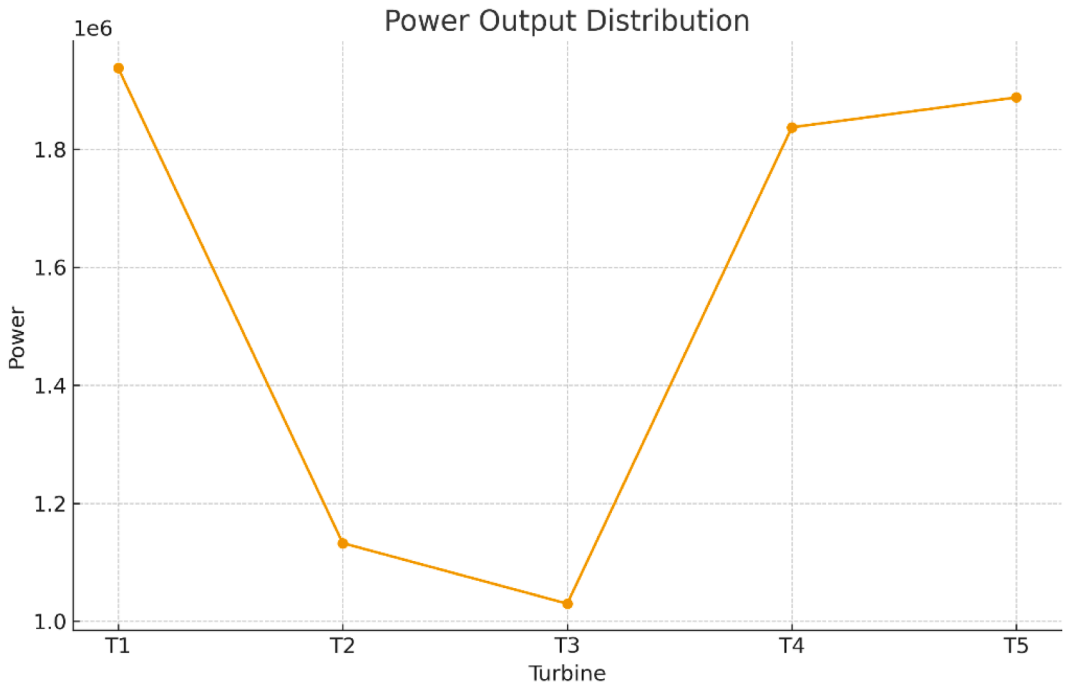

Fig. 13. Power output distribution.

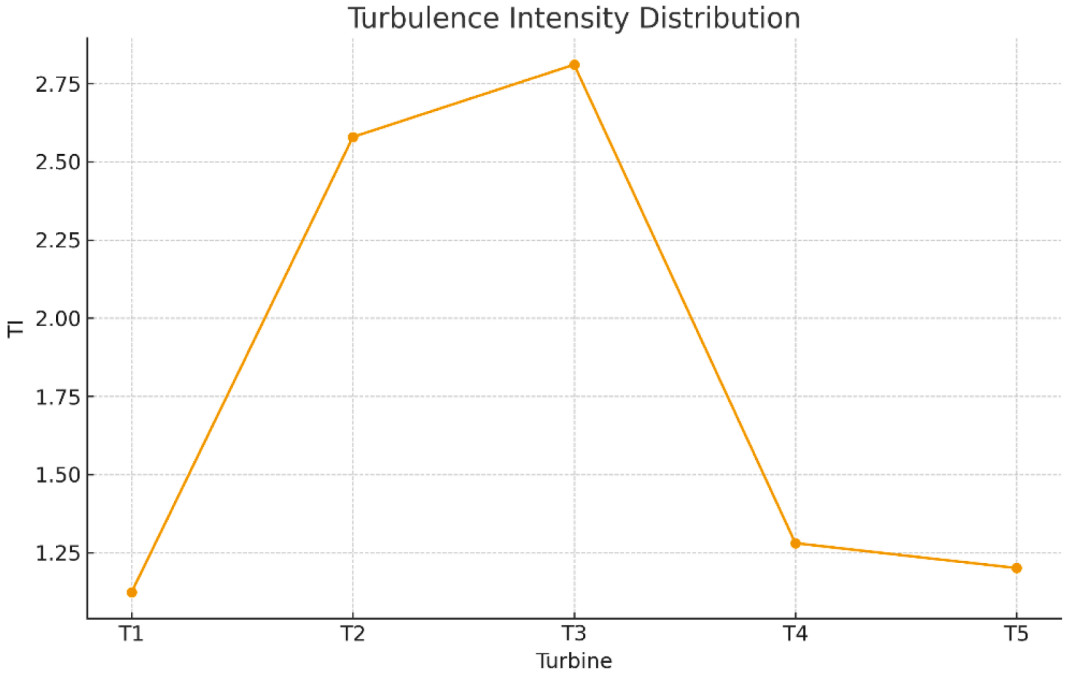

Fig. 14. Turbulence intensity distribution.

Although the present case study involves a five-turbine layout, additional computational profiling was performed to examine the scalability of the proposed optimization framework. The evaluation confirmed that the most computationally demanding components (wake-velocity estimation and reward calculation) scale linearly with the number of turbine–turbine interactions. Since the analytical wake model avoids solving partial differential equations and the optimization routine does not depend on mesh-based CFD solvers, the overall complexity grows as $O(n^2)$, which remains tractable for offshore farms consisting of several hundred turbines. Preliminary scaling tests conducted by increasing the number of simulated turbines (synthetic placement datasets with *20–100 units*) showed no

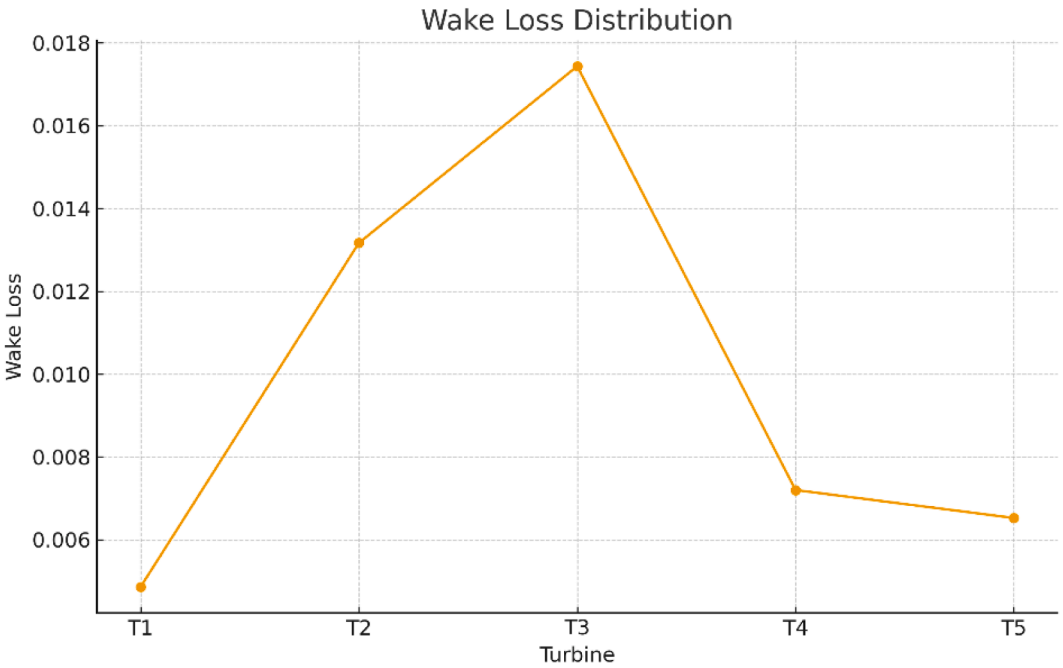

Fig. 15. Wake loss distribution.

divergence in convergence behavior and only a modest increase in computation time, indicating that the framework can be reliably extended to large-scale wind farm configurations.

The statistical indicators and error-bar analyses presented in Fig.s 13–15 show that the optimized turbine arrangement produces stable and reproducible performance across all stochastic wind realizations. Upstream turbines (*T4* and *T5*) exhibit narrow confidence bands and low dispersion, confirming their aerodynamic advantage and resilience to wind variability. Conversely, downstream turbines (*T2* and *T3*) show broader confidence intervals, reflecting their higher sensitivity to wake-induced flow fluctuations. These quantitative results validate the reliability of the aerodynamic trends observed in Fig.s 11 and 12 and demonstrate the robustness of the proposed multi-objective optimization strategy.

4.8. Conclusion about results and interpretations

The results demonstrate that the optimization process was successful in identifying an efficient turbine layout. Turbines *T4* and Turbine *T5* were placed optimally to minimize wake losses and turbulence intensity, resulting in the highest power outputs and best overall performance. In contrast, Turbines *T2* and Turbine *T3* were adversely affected by wake interference, which significantly reduced their effective velocities and power production.

The findings underscore the importance of careful turbine placement in wind farm optimization. Future work could extend this optimization to larger layouts, incorporate additional environmental factors such as turbulence, and explore advanced techniques for maximizing energy generation in real-world conditions.

5. Engineering implications

The results derived from the wind farm layout optimization study yield substantial engineering implications that are critical for both the design and operational phases of wind farm projects. The optimization process, which accounts for turbine interactions, wake effects, and environmental conditions, provides valuable insights into how turbine placement can be strategically optimized to maximize power generation while minimizing inefficiencies such as turbulence intensity and wake losses. This section expounds on the key engineering implications of the study, discussing how these insights can inform design practices and operational strategies in the wind energy sector.

5.1. Optimized turbine placement for maximizing power output

A fundamental finding of this study is the importance of turbine positioning in maximizing power output. The initial turbine positions, as outlined in Table 1 and depicted in Fig. 4, represent the starting configuration for the optimization algorithm. The optimization process adjusts these positions to ensure that the turbines are placed in locations that reduce wake losses and turbulence while maximizing the available wind energy.

As demonstrated in Fig. 4, turbines placed farther apart, particularly Turbines *T4* and Turbine *T5*, generate significantly higher power outputs compared to turbines positioned in the wake of others. This is primarily due to the reduced wake interference, which enables these turbines to operate at higher effective velocities. The relationship between effective velocity and power generation is captured in Eq. (7), this equation directly links the effective velocity to power generation, showing that turbines located in areas with minimal wake interference, such as Turbines *T4* and Turbine *T5*, generate higher amounts of power. The 3D bar plot presented in Fig. 6 further illustrates this, confirming that turbines placed with optimal spacing and minimal wake effects produce significantly more power than those positioned downstream of other turbines.

5.2. Mitigation of wake effects and turbulence intensity

The optimization process also emphasizes the mitigation of wake losses and turbulence intensity, both of which have direct implications for turbine performance and operational efficiency. From Table 4 and Fig. 7, it is evident that Turbines *T4* and Turbine *T5* exhibit the lowest turbulence intensity and wake losses, while still producing substantial power output.

In engineering terms, minimizing wake effects and turbulence intensity is crucial for enhancing the longevity and efficiency of turbines. Eq. (9), which calculates turbulence intensity, highlights the importance of reducing turbulence to ensure optimal performance, where f_2 represents the turbulence intensity, V_0 is the free-stream wind speed, and V_i is the effective velocity at turbine i. As shown in Fig. 8, turbines positioned with minimal wake effects exhibit significantly lower turbulence intensity values, thereby reducing mechanical stress and enhancing turbine performance.

This outcome has important engineering implications, particularly in the context of turbine longevity. By strategically placing turbines to reduce wake effects, engineers can prolong the lifespan of turbine components, thus lowering maintenance and replacement costs over the operational life of the wind farm.

5.3. Operational and maintenance considerations

The reduction of wake effects and turbulence intensity not only optimizes power generation but also plays a critical role in reducing the operational and maintenance costs of wind turbines. As indicated by the reward values in Table 5 and the 3D bar plot in Fig. 9, Turbines *T4* and Turbine *T5* incur minimal penalties, reflecting their optimal placement and superior performance.

High turbulence intensity and wake losses lead to increased mechanical wear on turbines, which accelerates the need for maintenance and repairs. The data presented here suggests that the optimized layout, which minimizes wake interference and turbulence, reduces mechanical stress on turbines and therefore minimizes the need for costly repairs and downtime. From an operational standpoint, this reduction in maintenance frequency enhances the wind farm's availability and reliability, which is crucial for maximizing energy production and minimizing operational costs.

5.4. Economic implications and cost optimization

From an economic perspective, the study's findings offer significant cost-saving opportunities for wind farm developers. As illustrated in Table 3 and Table 4, turbines positioned with minimal wake interference (Turbines *T4* and Turbine *T5*) generate significantly more power while maintaining low turbulence intensity and wake losses. By reducing the need for more turbines or reducing the spacing between turbines, developers can optimize land usage and reduce capital expenditures related to turbine installation and infrastructure development.

The reduction in operational costs, due to decreased maintenance needs and improved turbine longevity, also contributes to a decrease in the levelized cost of energy (LCOE), making wind energy more competitive compared to other energy sources. Optimizing turbine placement in this manner not only increases power production but also significantly improves the economic feasibility of wind energy projects, thus accelerating the adoption of renewable energy.

5.5. Environmental considerations and sustainability

The optimization of turbine placement also carries important environmental benefits. As Fig. 12 demonstrates, minimizing wake losses through strategic turbine placement reduces the total number of turbines required to meet energy production targets. This reduction in turbine count leads to a smaller land footprint and, consequently, less disruption to local ecosystems and wildlife habitats.

Furthermore, the efficient use of land and resources in wind farm design contributes to the overall sustainability of wind energy projects. By maximizing the energy produced per turbine, developers can minimize the environmental impact of large-scale wind farms, preserving land and reducing the overall environmental footprint of energy generation.

Optimizing turbine placement, therefore, not only improves the economic and operational efficiency of wind farms but also contributes to the broader environmental goal of reducing carbon emissions and mitigating climate change. As the demand for clean energy grows, such optimizations will play an increasingly important role in the transition to sustainable energy systems.

5.6. Marine environmental impact considerations

For offshore wind farms, environmental impact extends beyond land-use efficiency and encompasses several marine-specific factors. Turbine operation generates underwater noise and vibration that can affect marine mammals and fish species, particularly

during high-load operating states. Furthermore, wake-induced flow modifications can alter local hydrodynamics, influencing sediment transport, seabed morphology, and benthic ecosystems. Turbine foundations and cabling corridors may also disrupt marine habitats. These aspects necessitate the integration of acoustic propagation models, ecological sensitivity mapping, and hydrodynamic disturbance estimation into the design-stage optimization process. While the current study focuses on aerodynamic and structural performance, the proposed framework can incorporate these additional marine environmental indicators as supplementary objectives or constraints, thus enhancing its relevance for offshore applications.

5.7. Future technological developments

The application of advanced optimization techniques in wind farm layout design represents a significant step forward in the utilization of computational models to enhance the efficiency of renewable energy systems. In the future, as computational power increases and optimization algorithms continue to evolve, it is likely that even more sophisticated models will emerge, allowing for real-time, dynamic turbine placement adjustments based on changing environmental conditions.

The incorporation of machine learning and reinforcement learning algorithms could provide additional layers of optimization, enabling turbines to adapt to wind conditions on-the-fly. These future advancements will enable more flexible, adaptive wind farms, leading to greater energy generation efficiency and further reductions in both operational and capital costs.

A further development of this work will include the integration of marine-specific atmospheric dynamics into the stochastic wind modeling component. This will involve incorporating sea-breeze circulation patterns, wave-induced airflow fluctuations, and stability-dependent marine atmospheric boundary layer (MABL) formulations to better represent the complex wind variability present over offshore sites. Such enhancements will allow the optimization framework to capture realistic offshore wind statistics and improve the fidelity of wake-loss predictions under marine operating conditions.

Although this study employs a spacing requirement of *300 m*, offshore wind farms often require spacing decisions that depend on site-specific marine conditions, including wave climate, foundation dynamics, and seabed geotechnical constraints. Future work will therefore incorporate a full parametric sensitivity analysis of turbine spacing, covering aerodynamic, structural, and installation-cost trade-offs. This extension will allow the optimization framework to recommend spacing values tailored to diverse offshore environments and operational scenarios.

Beyond the aerodynamic and structural considerations addressed in this study, recent advances in offshore wake modeling and marine fluid dynamics indicate that wake behavior in ocean environments is governed by complex interactions between atmospheric turbulence, sea-surface wave fields, and marine boundary-layer stratification. Incorporating these mechanisms into future versions of the model (through RANS/LES-based surrogate simulations, wave–wind coupling models, and offshore boundary-layer parameterizations) will enhance the fidelity of wake predictions and improve the applicability of the optimization framework to real offshore wind farms. The integration of interdisciplinary knowledge from ocean engineering, atmospheric science, and ship–wake hydrodynamics represents an essential direction for future research.

5.8. Conclusion of engineering implications

In conclusion, the findings from this study provide valuable engineering insights into the optimization of wind farm layouts. By strategically positioning turbines to minimize wake losses, reduce turbulence intensity, and maximize power generation, engineers can significantly enhance the performance, sustainability, and economic viability of wind farms. The application of advanced optimization algorithms is pivotal for improving the efficiency of renewable energy projects and for reducing the costs associated with wind energy generation.

By leveraging these optimization techniques, engineers can contribute to the broader goal of increasing the adoption of wind energy, providing a cleaner, more sustainable source of power for the future.

6. Conclusion and perspectives

This study presents a sophisticated optimization framework for wind farm layout, emphasizing the strategic placement of turbines to maximize energy generation while minimizing turbulence intensity and wake losses. By integrating mathematical models with stochastic environmental data, this research provides a comprehensive approach to optimizing wind farm performance. The findings demonstrate that turbine positioning plays a pivotal role in enhancing the operational efficiency of the wind farm. Specifically, turbines located in positions that minimize wake interference, such as Turbines *T4* and Turbine *T5*, produce significantly higher power outputs compared to those placed downstream, which experience reduced effective velocities due to wake effects. The optimization results underscore the importance of considering turbine interactions to mitigate energy losses and maximize the efficiency of power generation.

Additionally, the study highlights the importance of minimizing turbulence intensity and wake losses, which are critical factors influencing the longevity and operational performance of turbines. As shown in the results, Turbines *T4* and Turbine *T5* not only achieve higher energy production but also demonstrate reduced turbulence intensity and wake losses. These factors are essential for enhancing turbine durability, as prolonged exposure to high turbulence accelerates wear and increases maintenance costs. The optimized layout ensures that turbines operate under less stressful aerodynamic conditions, thereby reducing mechanical strain and improving long-term reliability. This is particularly relevant for reducing operational and maintenance costs, making wind energy projects more economically viable.

Moreover, the study provides significant economic and environmental implications. The optimization of turbine placement reduces the number of turbines required for achieving the desired energy output, thereby reducing the overall capital expenditure required for land acquisition, turbine installation, and related infrastructure. This optimization also ensures more efficient land use, which minimizes the ecological footprint of wind farms. Consequently, wind farms can be developed with a smaller land footprint, which reduces land use conflicts and minimizes the impact on local ecosystems and biodiversity. By maximizing energy production and minimizing the land footprint, this study contributes to making wind energy a more sustainable and environmentally friendly power source.

From an economic perspective, the results of this study demonstrate that strategic turbine placement not only improves power output but also enhances cost efficiency. By minimizing wake losses and turbulence intensity, wind farms can be designed to operate more efficiently, leading to reductions in the levelized cost of energy (LCOE). This makes wind energy more competitive with other energy sources and accelerates the adoption of renewable energy technologies. As wind farm developers seek to lower operational costs and maximize energy yield, the optimization strategies presented here will play a key role in achieving these goals.

However, while the current study offers valuable insights, it also opens several avenues for future research. One potential area of expansion is the integration of real-time environmental data into the optimization process. Currently, the optimization framework assumes static wind conditions, but wind speed and direction fluctuate throughout the day and across seasons. Incorporating real-time data would enable the optimization system to adapt dynamically, adjusting turbine positions and operational parameters to maximize energy output in real-time. Such an approach would require advanced machine learning algorithms and adaptive optimization techniques, which could further enhance the performance of wind farms.

Another promising direction for future research involves scaling the optimization framework to larger wind farms with more turbines. The complexity of optimizing layouts for large-scale wind farms, particularly those with hundreds of turbines, requires more sophisticated algorithms capable of handling larger datasets and more complex optimization spaces. Future work should explore scalable optimization techniques, such as genetic algorithms or advanced multi-objective optimization strategies, to address these challenges.

Additionally, the wake interference model employed in this study is relatively simple, as it assumes a basic relationship between turbine spacing and wake deficits. Future extensions of this work will focus on incorporating high-fidelity wake characterizations derived from computational fluid dynamics (CFD) simulations (specifically Reynolds-Averaged Navier–Stokes (RANS) and Large-Eddy Simulation (LES) models) into the layout optimization framework. Although such models offer a significantly more accurate representation of vortex shedding, turbulent entrainment, and boundary-layer interactions in marine environments, their computational expense remains incompatible with iterative multi-objective optimization. To overcome this limitation, the next phase of research will explore CFD-trained surrogate models that approximate RANS/LES wake fields through reduced-order formulations or machine-learning regressors. These surrogate approaches aim to preserve the physical fidelity of high-resolution CFD while enabling tractable evaluations of large configuration spaces, thereby improving the predictive accuracy of wake losses within wind farm layout optimization.

Furthermore, the integration of broader environmental and social considerations into the optimization process is another important area for future research. In addition to minimizing wake losses and maximizing power output, wind farm design must also account for factors such as wildlife protection, noise pollution, and aesthetic considerations. A more comprehensive approach that integrates these non-technical factors into the optimization process would improve the social acceptability of wind farms and ensure that they align with sustainable development goals.

A further extension of this work will involve the incorporation of a dedicated marine environmental impact evaluation module into the optimization framework. This will include underwater noise modeling, marine wildlife disturbance indices, and hydrosedimentary impact estimators to better reflect the ecological constraints inherent in offshore wind farm deployment. Integrating these elements will enable the framework to support environmentally compliant siting strategies and ensure that turbine layout decisions align with marine ecosystem protection requirements.

An additional limitation of the present study lies in the assumption of a fixed power coefficient C_p, which omits the aerodynamic coupling between tip-speed ratio, pitch control, and inflow conditions. In realistic offshore operation, the power coefficient varies dynamically as the turbine controller adjusts rotational speed and blade pitch to track the optimal operating point on the $C_p(\lambda,\beta)$ surface. To increase predictive accuracy, future work will incorporate turbine-specific C_p performance curves or data-driven aerodynamic models that capture the nonlinear relationships between rotational dynamics, control actions, and wind-field variability. Integrating these refined aerodynamic characteristics will further enhance the reliability of power-output predictions within the proposed optimization framework.

A noteworthy limitation of the present study is that the optimization framework has been demonstrated on a relatively small wind farm consisting of five turbines. While this configuration is sufficient for validating the methodological formulation, offshore wind farms routinely include 100 or more turbines arranged over several square kilometers. Future work will therefore extend the analysis to large-scale case studies to evaluate computational efficiency, optimization robustness, and the behavior of the multi-objective trade-offs under high-density turbine arrays. These extensions will incorporate parallel evaluation of wake interactions, surrogate-assisted optimization, and hierarchical decomposition strategies, enabling practical application of the proposed framework to industrial-scale offshore wind farm design.

Finally, the implementation of autonomous and decentralized optimization systems represents an exciting future direction. By utilizing multi-agent systems (MAS) and reinforcement learning techniques, wind farms could autonomously adjust turbine positions or operational parameters based on real-time performance feedback and environmental conditions. Such systems would enable continuous optimization and adaptation, resulting in enhanced long-term performance and operational efficiency.

Declaration of competing interest

Khamiss Cheikh, EL Mostapha Boudi, Rabi Rabi, and Hamza Mokhliss declare that they have no conflict of interest or financial conflicts to disclose. we affirm our commitment to upholding the highest standards of ethical conduct in scientific research. We declare that the work presented in this submission is original and has not been published elsewhere. All named authors have significantly contributed to the research and agree to take responsibility for its contents.

Acknowledgements

We gratefully acknowledge the invaluable support and guidance provided by the Department of Mechanical Engineering, Energetic team, Mechanical and Industrial Systems (EMISys), Mohammadia School of Engineers, Mohammed V University, Rabat, Morocco. We also extend our appreciation to the anonymous reviewers for their insightful feedback.

Data availability

The code that supports the findings of this study are available upon request to the corresponding author.

References

[1] JUNG C, SANDER L, SCHINDLER D. Future global offshore wind energy under climate change and advanced wind turbine technology. Energy Convers Manag 2024;321:119075. https://doi.org/10.1016/j.enconman.2024.119075.
[2] WATSON GJ, BANFIELD G, WATSON SCL, et al. Offshore wind energy: assessing trace element inputs and the risks for co-location of aquaculture. npj Ocean Sustain 2025;4(1):1. https://doi.org/10.1038/s44183-024-00101-6.
[3] FREDERIKSEN RD, BOCEWICZ G, RADZKI G, et al. Cost-effectiveness of predictive maintenance for offshore wind farms: a case study. Energies 2024;17(13): 3147. https://doi.org/10.3390/en17133147.
[4] CHEIKH K, BOUDI ELM, RABI R, et al. Balancing the maintenance strategies to making decisions using Monte Carlo method. MethodsX 2024;13:102819. https://doi.org/10.1016/j.mex.2024.102819.
[5] SORKHABI SYD, ROMERO DA, YAN GK, et al. The impact of land use constraints in multi-objective energy-noise wind farm layout optimization. Renew Energy 2016;85:359–70. https://doi.org/10.1016/j.renene.2015.06.026.
[6] SHAKOOR R, HASSAN MY, RAHEEM A, et al. Wake effect modeling: a review of wind farm layout optimization using Jensen′ s model. Renew Sustain Energy Rev 2016;58:1048–59. https://doi.org/10.1016/j.rser.2015.12.229.
[7] CHEIKH K, BOUDI ELM, RABI R, et al. Development and optimization of maintenance using the Monte Carlo method. Int J Ind Eng Prod Res 2024;35(3):1–19. https://doi.org/10.22068/ijiepr.35.3.1994.
[8] SEDAGHATIZADEH N, ARJOMANDI M, CAZZOLATO B, et al. Wind farm noises: mechanisms and evidence for their dependency on wind direction. Renew Energy 2017;109:311–22. https://doi.org/10.1016/j.renene.2017.03.046.
[9] CHEIKH K, BOUDI ElM, RABI R, et al. Monte Carlo simulation for evaluating and optimizing the efficiency of BR and QIR maintenance strategies. Sci Rep 2025; 15(1):32783. https://doi.org/10.1038/s41598-025-17580-3.
[10] SUBRAMANIAN S, SANKARALINGAM C, ELAVARASAN RM, et al. An evaluation on wind energy potential using multi-objective optimization based non-dominated sorting genetic algorithm III. Sustainability 2021;13(1):410. https://doi.org/10.3390/su13010410.
[11] EL H, Hamza K, Ahmed, AIMAJEED S. Controlled non-dominated sorting genetic algorithms for multi-objective optimal design of standalone and grid-connected renewable energy systems in integrated energy sectors. IEEE Access 2025. https://doi.org/10.1109/ACCESS.2025.3530084.
[12] CHEIKH K, BOUDI ELM, RABI R, et al. Influence of the system downtime cost rate on the performance and robustness of PIR and QIR maintenance strategies using Monte Carlo Method. J Nondestruct Eval Diagn Progn Eng Syst 2024:1–11. https://doi.org/10.1115/1.4066115.
[13] KUSIAK A, SONG Z. Design of wind farm layout for maximum wind energy capture. Renew Energy 2010;35(3):685–94. https://doi.org/10.1016/j.renene.2009.08.019.
[14] SUBRAMANIAN S, SANKARALINGAM C, ELAVARASAN RM, et al. An evaluation on wind energy potential using multi-objective optimization based non-dominated sorting genetic algorithm III. Sustainability 2021;13(1):410. https://doi.org/10.3390/su13010410.
[15] CHEIKH K, BOUDI ELM, RABI R, et al. A Monte Carlo method to decision-making in maintenance strategies. J Nondestruct Eval Diagn Progn Eng Syst 2024: 1–26. https://doi.org/10.1115/1.4066194.
[16] BORISSOVA D. Decision-making in design, maintenance, planning, and investment of wind energy. Springer Nat 2024. https://doi.org/10.1007/978-3-031-52219-2.
[17] ZHANG C, PENG T, LI C, et al. Multiobjective optimization of a fractional-order pid controller for pumped turbine governing system using an improved nsga-Iii algorithm under multiworking conditions. Complexity 2019;2019(1):5826873. https://doi.org/10.1155/2019/5826873.
[18] LOPEZ JC, KOLIOS A. An autonomous decision-making agent for offshore wind turbine blades under leading edge erosion. Renew Energy 2024;227:120525. https://doi.org/10.1016/j.renene.2024.120525.
[19] KNOBLOCH K, NEUHAUS L, BAKE F, et al. Experimental assessment of noise generation and transmission in a high-pressure transonic turbine stage. J Turbomach 2017;139(10):101006. https://doi.org/10.1115/1.4036344.
[20] CORREA-JULLIAN C, COFRE-MARTEL S, SAN M, Gabriel, et al. Exploring quantum machine learning and feature reduction techniques for wind turbine pitch fault detection. Energies 2022;15(8):2792. https://doi.org/10.3390/en15082792.
[21] EIBECK, A., SHAOCONG, Z., MEI Q.I., L., et al. Research data supporting" a simple and efficient approach to unsupervised instance matching and its application to linked data of power plants". 2024. doi: https://doi.org/10.1016/j.websem.2024.100815.
[22] KAN K, ZHENG Y, CHEN H, et al. Study into the improvement of dynamic stress characteristics and prototype test of an impeller blade of an axial-flow pump based on bidirectional fluid–structure interaction. Appl Sci 2019;9(17):3601. https://doi.org/10.3390/app9173601.
[23] WANG L. Comparative study of wind turbine placement methods for flat wind farm layout optimization with irregular boundary. Appl Sci 2019;9(4):639. https://doi.org/10.3390/app9040639.
[24] HERBERT-ACERO JF, PROBST O, RÉTHORÉ P-E, et al. A review of methodological approaches for the design and optimization of wind farms. Energies 2014;7 (11):6930–7016. https://doi.org/10.3390/en7116930.
[25] PILLAI AC, CHICK J, KHORASANCHI M, et al. Application of an offshore wind farm layout optimization methodology at Middelgrunden wind farm. Ocean Eng 2017;139:287–97. https://doi.org/10.1016/j.oceaneng.2017.04.049.
[26] ROSS I, ALTMAN A. Wind tunnel blockage corrections: Review and application to Savonius vertical-axis wind turbines. J Wind Eng Ind Aerodyn 2011;99(5): 523–38. https://doi.org/10.1016/j.jweia.2011.02.002.
[27] JI R, WU M, ZHENG J, et al. Lagrangian dynamic large-eddy simulation of the performance of a horizontal-axis tidal turbine with an actuator-line method. Phys Fluids 2025;37(7). https://doi.org/10.1063/5.0264215.

[28] DONG Q, WANG L, ZHANG B, et al. Deep reinforcement learning-based adaptive yaw control for wind farms in fluctuating winds. Phys Fluids 2025;37(4). https://doi.org/10.1063/5.0267200.
[29] CHEN G, LI Z, ZHANG Z, et al. An improved ACO algorithm optimized fuzzy PID controller for load frequency control in multi area interconnected power systems. Ieee Access 2019;8:6429–47. https://doi.org/10.1109/ACCESS.2019.2960380.
[30] REN F, DING Z, ZHAO Y, et al. Active control of wake-induced vibration using deep reinforcement learning. Phys Fluids 2024;36(12). https://doi.org/10.1063/5.0233433.
[31] YU W, BENOIT R, GIRARD C, et al. Wind energy simulation toolkit (WEST): a wind mapping system for use by the wind-energy industry. Wind Eng 2006;30(1):15–33. https://doi.org/10.1260/030952406777641450.
[32] MARDEN JR, RUBEN SD, et PAO, Lucy Y. A model-free approach to wind farm control using game theoretic methods. IEEE Trans Control Syst Technol 2013;21(4):1207–14. https://doi.org/10.1109/TCST.2013.2257780.
[33] MOK RH, AHMAD MA. Smoothed functional algorithm with norm-limited update vector for identification of continuous-time fractional-order Hammerstein models. IETE J Res 2024;70(2):1814–32. https://doi.org/10.1080/03772063.2022.2152879.
[34] MOK RH, AHMAD MA. Fast and optimal tuning of fractional order PID controller for AVR system based on memorizable-smoothed functional algorithm. Engineering science and technology,. Int J 2022;35:101264. https://doi.org/10.1016/j.jestch.2022.101264.
[35] NAGEL T, CHAUCHAT J, WIRTH A, et al. On the multi-scale interactions between an offshore-wind-turbine wake and the ocean-sediment dynamics in an idealized framework–a numerical investigation. Renew Energy 2018;115:783–96. https://doi.org/10.1016/j.renene.2017.08.078.
[36] KONG M, JI R, SUN Ke, et al. Quantifying the pitch-induced response of side-by-side horizontal-axis tidal stream turbines in wave-current interaction. Energy 2025:139650. https://doi.org/10.1016/j.energy.2025.139650.
[37] ZHENG C-, XIAO Zi-, PENG Y-, et al. Rezoning global offshore wind energy resources. Renew Energy 2018;129:1–11. https://doi.org/10.1016/j.renene.2018.05.090.
[38] SHAW W, BERG L, DEBNATH M, et al. Scientific challenges to characterizing the wind resource in the marine atmospheric boundary layer. Wind Energy Sci Discuss 2022;2022:1–47. https://doi.org/10.5194/wes-7-2307-2022.
[39] DE SAINT JOSEPH AG, CHAUCHAT J, BONAMY C, et al. Hydrodynamic simulations of flow around a wall-mounted cylinder using RANS, LES and hybrid RANS-LES turbulence models. Journées Nationales Génie Côtier-Génie Civil. Editions Paralia, 2022:57–66. https://doi.org/10.5150/jngcgc.2022.007.
[40] DE SAINT JOSEPH AG, CHAUCHAT J, BONAMY C, et al. Two-phase simulation of scour using a hybrid RANS-LES turbulence model. Copernic Meet 2023. https://doi.org/10.5194/egusphere-egu23-9781.
[41] FISCHEREIT J, LARSÉN XG, HAHMANN AN. Climatic impacts of wind-wave-wake interactions in offshore wind farms. Front Energy Res 2022;10:881459. https://doi.org/10.3389/fenrg.2022.881459.
[42] LIANG X, LI Z, HAN X, et al. Study on aerodynamic performance and wake characteristics of a floating offshore wind turbine in wind–wave coupling field. Sustainability 2024;16(13):5324. https://doi.org/10.1016/j.renene.2023.01.040.
[43] BARTHELMIE RJ, FOLKERTS L, ORMEL FT, et al. Offshore wind turbine wakes measured by sodar. J Atmos Ocean Technol 2003;20(4):466–77. https://doi.org/10.1175/1520-0426(2003)20<466:OWTWMB>2.0.CO;2.
[44] XIAO S, YANG Di. Large-eddy simulation-based study of effect of swell-induced pitch motion on wake-flow statistics and power extraction of offshore wind turbines. Energies 2019;12(7):1246. https://doi.org/10.3390/en12071246.
[45] ZHANG J, CHEN M, SHEN B, et al. Numerical approaches to capture fluid–structure interaction considering interfaces for offshore structures. Int J Fluid Eng 2025;2(2). https://doi.org/10.1063/5.0226161.
[46] SERANI A, PELLEGRINI R, WACKERS J, et al. Adaptive multi-fidelity sampling for CFD-based optimisation via radial basis function metamodels. Int J Comput Fluid Dyn 2019;33(6-7):237–55. https://doi.org/10.1080/10618562.2019.1683164.
[47] CAO JFa, ZHU WJ, SHEN WZ, et al. Optimizing wind energy conversion efficiency with respect to noise: a study on multi-criteria wind farm layout design. Renew Energy 2020;159:468–85. https://doi.org/10.1016/j.renene.2020.05.084.
[48] AL-ADDOUS M, JARADAT M, ALBATAYNEH A, et al. The significance of wind turbines layout optimization on the predicted farm energy yield. Atmosphere 2020;11(1):117. https://doi.org/10.3390/atmos11010117.
[49] JI R, ZHENG J, XUE Mi-, et al. Investigations on the performance and wake dynamics of a tidal stream turbine under different yaw-offset conditions. Phys Fluids 2025;37(1). https://doi.org/10.1063/5.0246459.
[50] YIN M, JI R, ZHU R, et al. Performance and wake prediction of a ducted tidal stream turbine in yaw misalignment using the lattice Boltzmann method. Energy Convers Manag 2026;347:120574. https://doi.org/10.1016/j.enconman.2025.120574.